



# Random effects inducing heart pathological dynamics: An approach based on mathematical models

Augusto Cheffer, Marcelo A. Savi<sup>\*</sup>

Universidade Federal do Rio de Janeiro, COPPE, Department of Mechanical Engineering, Center for Nonlinear Mechanics, P.O. Box 68.503, 21.941.972, Rio de Janeiro, RJ, Brazil

## ARTICLE INFO

### Keywords:

Nonlinear dynamics  
Chaos  
Cardiac rhythms  
Heart  
DDEs  
Random  
Poincaré maps

## ABSTRACT

This work deals with an investigation of randomness effects on heart rhythm analysis. A mathematical model composed by three-coupled nonlinear oscillators coupled by time-delayed connections is employed for this aim. In this regard, heart rhythm is governed by delayed-differential equations. Nondeterministic aspects are incorporated considering random connections among oscillators. The main idea is to show that nonlinearities and randomness define together the great variety of possibilities in the heart dynamical system. In general, results corroborate that the model is able to capture the main behaviors of the cardiac system showing that pathological behaviors can evolve from normal rhythms due to random couplings. Experimental data corroborate this argues pointing that nonlinear dynamical analysis is useful for a proper physiological comprehension.

## 1. Introduction

Rhythmic changes of cardiovascular measures indicate that heart behavior is related to a dynamical system where normal and pathological responses can be achieved by parametric changes. This comprehension points that heart arrhythmia represent dynamical diseases. The diversity of heart system possibilities is essentially related to its nonlinearities. Hence, heart nonlinear dynamics has an intrinsic richness associated with periodic, quasi-periodic and non-periodic responses that can be related to either normal or pathological physiological functioning.

There are different forms to evaluate the heart functioning by the measure of some signal. Electrocardiogram (ECG) is one of the most popular measurement that records the heart electrical activity. The electrical impulses of the heart functioning are recorded in the form of waves, which represents the electrical current in different areas of heart.

Heart rate variability (HRV) is one of the best predictors of arrhythmic events (Mansier et al., 1996). Some procedures include detection of R-peaks (Pan and Tompkins, 1985; Kaplan, 1990) and calculation of heart rate variability and breathing (Moody et al., 1985; Malik and Camm, 1995). HRV can be considerably different even in the absence of physical or mental stress and this information has been applied for clinical and research purposes. The existence of HRV points that, besides nonlinear characteristics, heart system can present some

random behavior.

Kantz and Schreiber (2002) established a comparison between deterministic chaos and random noise for the heart rhythm analysis. Bozoki (1997) developed a data acquisition method for fetal heart rate suitable to be used by both power spectral analysis (statistical) and chaos theory (deterministic). Kaplan and Cohen (1990) analyzed fibrillatory ECGs of dogs and results suggest that this fibrillation is similar to a random signal. However, an example is discussed showing that a deterministic dynamical system can generate random-looking, nonchaotic behavior. Yates and Benton (1994) exposed the difficulty to decide between deterministic or statistical analysis to treat human cardiovascular data. Aronis et al. (2018) applied symbolic analysis in atrial fibrillation surrogate data and results point that this is not driven by a rescaled linear stochastic process or a fractional noise. They supported the development of deterministic or nonlinear stochastic modeling. Son et al. (2019) presented a stochastic cardiovascular-pump model to represent the effects of left ventricular assist devices on heart hemodynamics. Based on that, both nonlinear and random aspects are essential for the comprehension of heart system dynamics.

Several studies analyzed influences of external factors on the HRV as the increase of physical effort or breathing. Glass (2009) discussed three main points: stochastic stimulus influences, respiratory influences and multiple feedback circuits. In a theoretical investigation of a modulation model of normal SA rhythm, Zhang et al. (2009) showed that the

<sup>\*</sup> Corresponding author.

E-mail addresses: [augusto.cheffer@poli.ufrj.br](mailto:augusto.cheffer@poli.ufrj.br) (A. Cheffer), [savi@mecanica.ufrj.br](mailto:savi@mecanica.ufrj.br) (M.A. Savi).

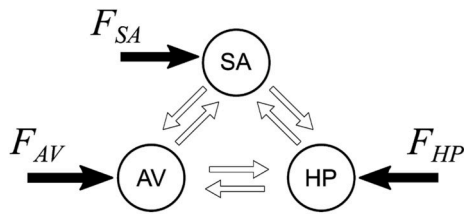


Fig. 1. Conceptual model of the general cardiac functioning.

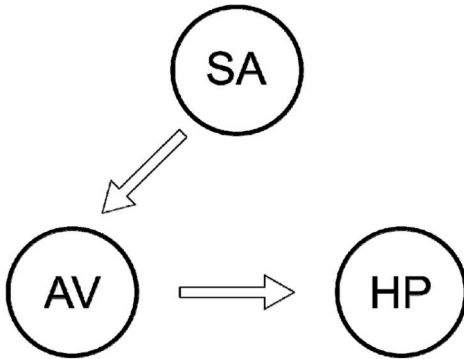


Fig. 2. Conceptual model of the normal heart functioning.

stochastic release of the acetylcholine regulator in the vicinity of the SA node leads to an irregular, chaotic rhythm. It is known that breathing influences heart rate in such a way that the heartbeat rate increases during inspiration and decreases on exhalation. [Wessel et al. \(2009\)](#) employed regression methods to investigate such coupling and concluded that the heart rate variability is directly caused by fluctuations on respiratory rate. [Buchner et al. \(2009\)](#) investigated the bidirectional coupling between respiration and cardiac rates using stochastic methods.

This paper investigates the influence of nondeterministic effects on cardiac system dynamics. The idea is to analyze situations where a heart rhythm can evolve from different rhythms due to random effects. A variation of the mathematical model proposed by [Gois and Savi \(2009\)](#) is employed to describe heart dynamics. This model considers three oscillators with delayed couplings. Each oscillator is described by a modified Van der Pol oscillator ([Van Der Pol and Van Der Mark, 1928](#)), presented on [Grudzinski and Zebrowski \(2004\)](#). The employed mathematical model can reproduce ECGs considering normal behavior and several pathologies. Random couplings are investigated showing that they can change the ongoing rhythm, inducing different pathologies. This can contribute to the understanding of physiological details of cardiac system behavior, which can motivate more efficient clinical strategies. In addition, it is possible to imagine applications related to the construction of artificial pacemakers and control of heart rhythms.

$$\dot{x}_1 = x_2$$

$$\dot{x}_2 = F_{SA}(t) - \alpha_{SA}x_2(x_1 - \nu_{SA1})(x_1 - \nu_{SA2}) - \frac{x_1(x_1 + d_{SA})(x_1 + e_{SA})}{d_{SA}e_{SA}} - k_{AV-SA}x_1 + k_{AV-SA}^{\tau}x_3^{\tau_{AV-SA}} - k_{HP-SA}x_1 + k_{HP-SA}^{\tau}x_5^{\tau_{HP-SA}}$$

$$\dot{x}_3 = x_4$$

$$\dot{x}_4 = F_{AV}(t) - \alpha_{AV}x_4(x_3 - \nu_{AV1})(x_3 - \nu_{AV2}) - \frac{x_3(x_3 + d_{AV})(x_3 + e_{AV})}{d_{AV}e_{AV}} - k_{SA-AV}x_3 + k_{SA-AV}^{\tau}x_1^{\tau_{SA-AV}} - k_{HP-AV}x_3 + k_{HP-AV}^{\tau}x_5^{\tau_{HP-AV}}$$

$$\dot{x}_5 = x_6$$

$$\dot{x}_6 = F_{HP}(t) - \alpha_{HP}x_6(x_5 - \nu_{HP1})(x_5 - \nu_{HP2}) - \frac{x_5(x_5 + d_{HP})(x_5 + e_{HP})}{d_{HP}e_{HP}} - k_{SA-HP}x_5 + k_{SA-HP}^{\tau}x_1^{\tau_{SA-HP}} - k_{AV-HP}x_5 + k_{AV-HP}^{\tau}x_3^{\tau_{AV-HP}}$$

(1)

Table 1  
Cardiac system parameters.

SA oscillator		HP oscillator	
$\alpha_{SA}$	3	$\alpha_{HP}$	7
$\nu_{SA1}$	1	$\nu_{HP1}$	1.65
$\nu_{SA2}$	-1.9	$\nu_{HP2}$	-2
$d_{SA}$	1.9	$d_{HP}$	7
$e_{SA}$	0.55	$e_{HP}$	0.67
AV oscillator		Couplings	
$\alpha_{AV}$	3	$k_{SA-AV}$	3
$\nu_{AV1}$	0.5	$k_{AV-HP}$	55
$\nu_{AV2}$	-0.5	$k_{SA-AV}^{\tau}$	3
$d_{AV}$	4	$k_{AV-HP}^{\tau}$	55
$e_{AV}$	0.67	Time delays	
		$\tau_{SA-AV}$	0.8
		$\tau_{AV-HP}$	0.1

After this introduction, the paper is organized as follows. Mathematical model is presented and numerical simulations are developed showing some heart behaviors, highlighting physiological aspects and their effects on ECG. Randomness effects on heart dynamics are evaluated by considering random coupling variables. Final remarks are presented in the sequence.

## 2. Mathematical modeling

Heart is a muscular organ activated by electrical stimuli with the function of pumping blood through all the organs and tissues of the body. The heart is divided into 4 cavities (2 atria and 2 ventricles) and its electrical activity can be understood as a network formed by sinoatrial node (SA), atrioventricular node (AV) and His-Purkinje (HP) complex ([Gois and Savi, 2009](#); [Glass, 2009](#)). The natural pacemaker is the SA node, where electrical activity starts, propagating as a wave to stimulate atria. Upon reaching the AV node, it initiates a pulse that excites the bundle of His, which in turn, transmits to the Purkinje fibers. Usually, the electrical impulses generated during cardiac functioning are recorded in the form of ECG.

Based on that, a cardiac model can be built from the coupling of nonlinear oscillators. [Gois and Savi \(2009\)](#) proposed the use of three oscillators (SA, AV and HP complex) with asymmetrical and bidirectional connections in order to build a general model that is capable of reproducing the cardiac behavior. [Fig. 1](#) shows the conceptual model that shows each one of the oscillators and the couplings among them.

By assuming that the oscillators are coupled by time-delayed terms that represent the transmitting time spent among each one of the oscillators, the cardiac system dynamics is governed by the following equations where indexes SA, AV and HP represents each oscillator and also their couplings.

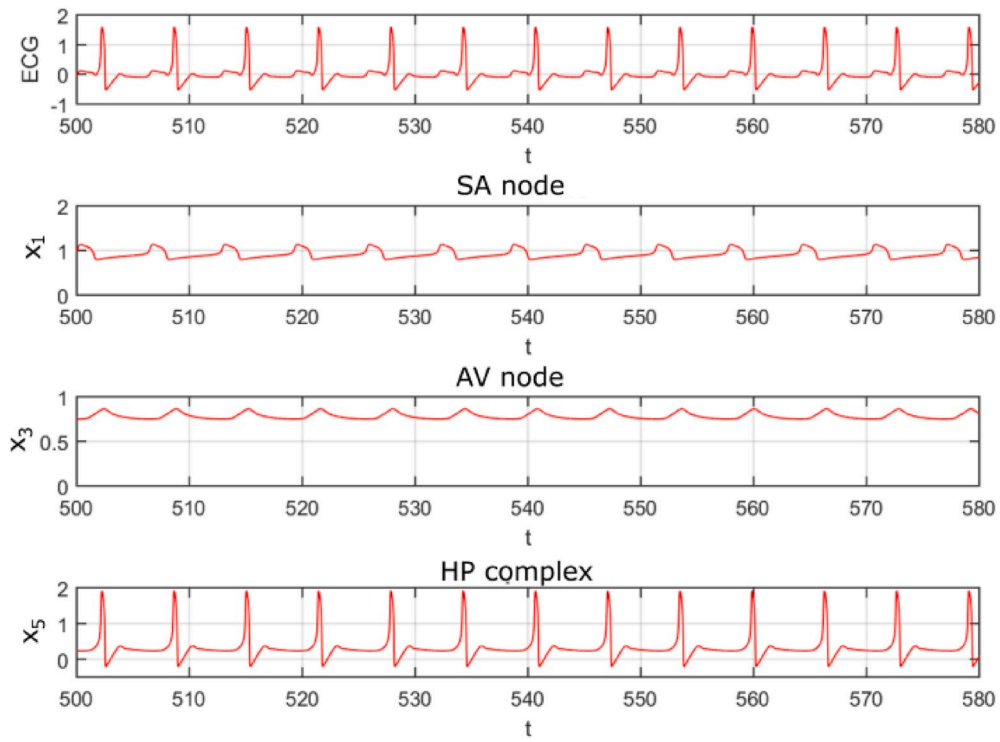
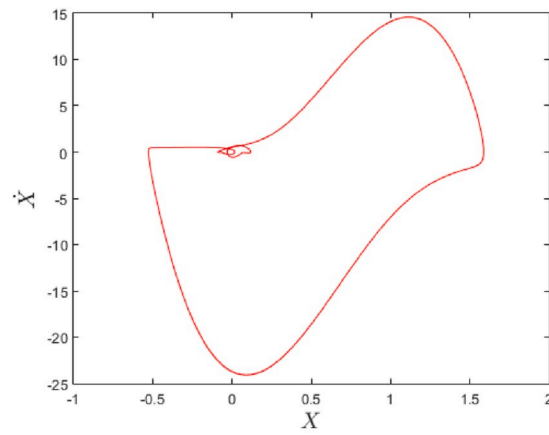
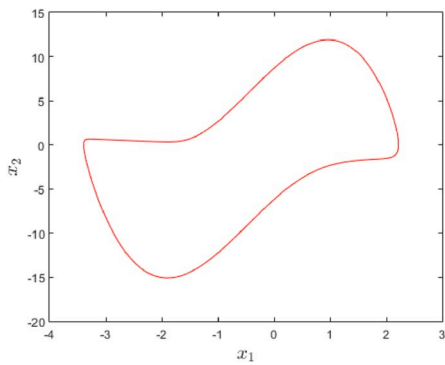


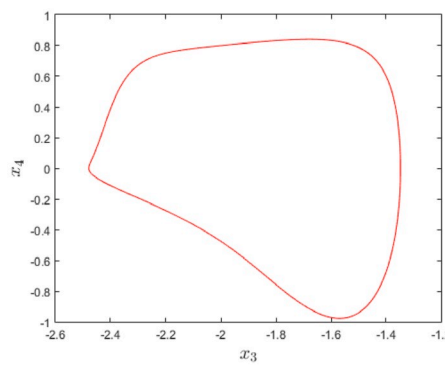
Fig. 3. Normal ECG representation and isolated oscillator responses.



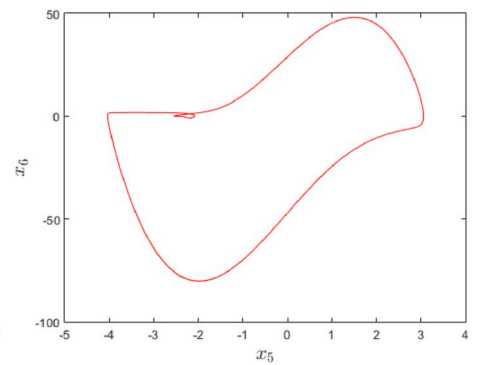
(a)



(b)



(c)



(d)

Fig. 4. Normal response. (a) ECG state space. (b) SA node state space. (c) AV node state space. (d) HP complex state space.

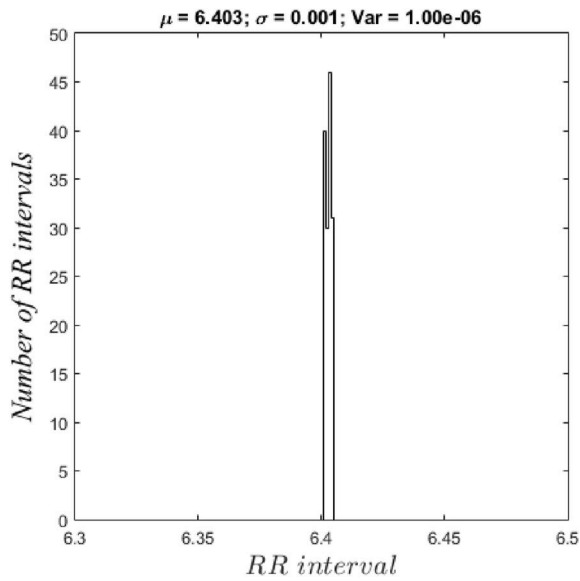


Fig. 5. R-R histogram for normal rhythm.

Assuming that indexes  $m$  and  $n$  can represent SA, AV or HP, and  $m \neq n$ ,  $\alpha_m$  defines the pulse shape, characterizing the time when the heart receives the stimulus;  $\nu_{m1}$  and  $\nu_{m2}$  determine the signal amplitude;  $k_{m-n}$  and  $k_{m-n}^r$  are coupling coefficients between  $m$  and  $n$  nodes; and  $x_i^{\tau_{m-n}} = x_i(t - \tau_{m-n})$  are delayed terms where  $\tau_{m-n}$  is the time delay. Since the couplings have temporal lags, the system is governed by delayed differential equations (DDEs). Besides,  $F_m(t) = \rho_m \sin(\omega_m t)$  is an external excitation that represents spatio-temporal stimulus and therefore, defines a reduced order representation of these spatio-temporal aspects, increasing the system dimension.

The ECG is formed by a combination of the signal of each one of the oscillators, being formed by a linear combination of the state variables given by (Gois and Savi, 2009).

$$X = ECG = \beta_0 + \beta_1 x_1 + \beta_2 x_3 + \beta_3 x_5 \quad (2)$$

where  $\beta_0, \beta_1, \beta_2$  and  $\beta_3$  are constants. Therefore,

$$\dot{X} = \frac{dECG}{dt} = \beta_1 x_2 + \beta_2 x_4 + \beta_3 x_6 \quad (3)$$

The fourth order Runge-Kutta method with linear interpolation of time-delayed variables is used to integrate system (3) (Mensour and Longtin, 1998). In order to treat the DDEs system, it is necessary to approximate their solutions in time instants before  $\tau_j$ . A Taylor series expansion is proposed (Cunningham, 1954; Gois and Savi, 2009).

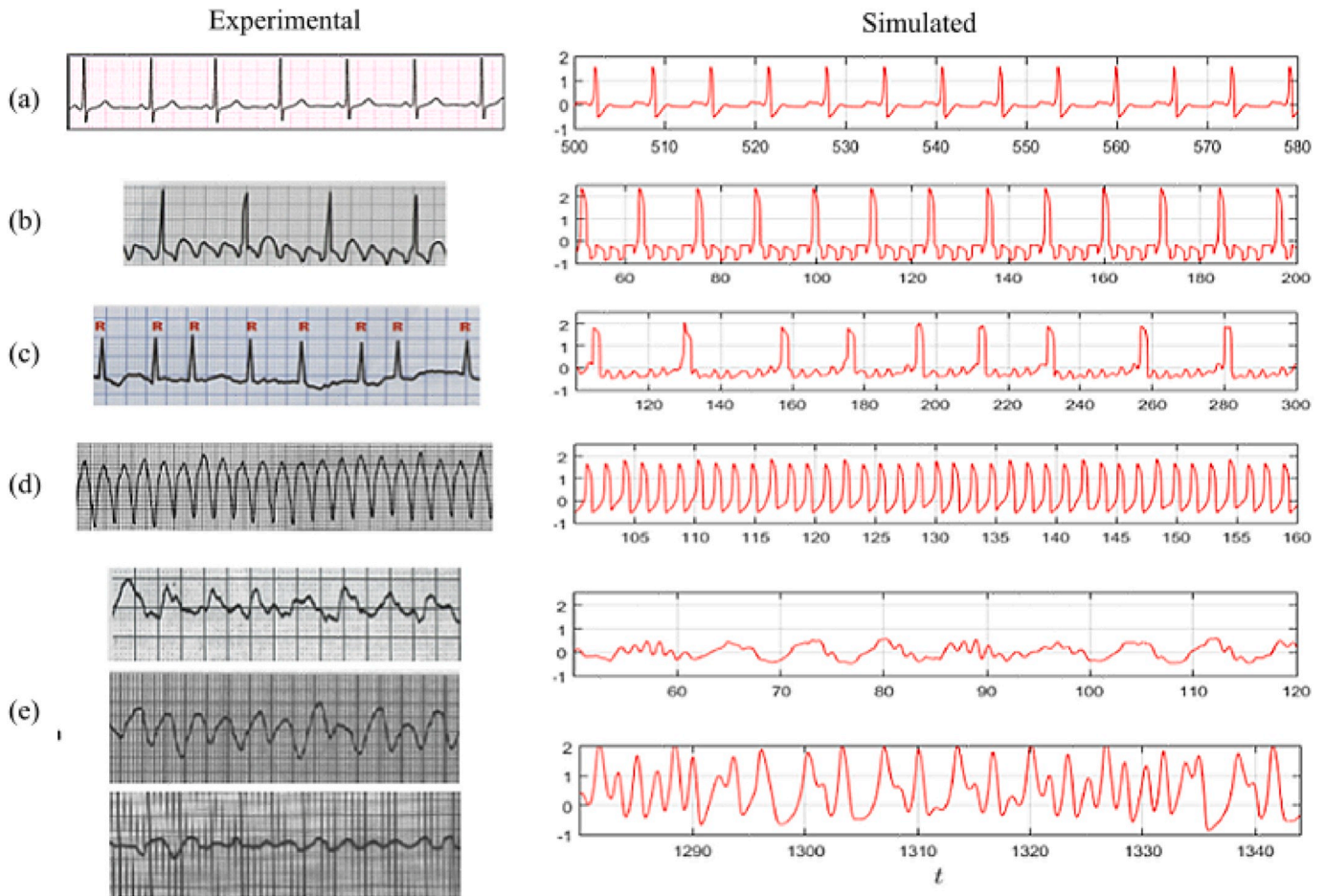


Fig. 6. Experimental e simulated ECG time series: (a) normal, (b) atrial flutter, (c) atrial fibrillation, (d) ventricular flutter and (e) different types of ventricular fibrillation.

**Table 2**  
Cardiac system parameters changed from normal rhythm to describe pathological behaviors.

	Atrial flutter	Atrial fibrillation	Ventricular flutter	Ventricular fibrillation with stimulus	Ventricular fibrillation without stimulus
<b>SA oscillator</b>					
$\nu_{SA_1}$	1.65	1	1	1	1
$\nu_{SA_2}$	- 4.2	- 1.9	- 1.9	- 1.9	- 1.9
<b>AV oscillator</b>					
$\alpha_{AV}$	7	7	3	3	3
<b>HP oscillator</b>					
$\alpha_{HP}$	7	7	7	0.5	0.5
<b>External Stimuli</b>					
$\rho_{SA}$	0	8	0	0	0
$\rho_{HP}$	0	0	0	30	0
$\omega_{SA}$	0	2.1	0	0	0
$\omega_{HP}$	0	0	0	0.8	0
<b>Couplings</b>					
$k_{SA-AV}$	0.66	0.66	3	3	3
$k_{AV-HP}$	14	14	45	30	14
$k_{SA-AV}^c$	0.02	0.09	3	3	0.4
$k_{AV-HP}^c$	60	38	20	30	38
$\tau_{SA-AV}$	0.66	0.8	0.8	0.8	0.8

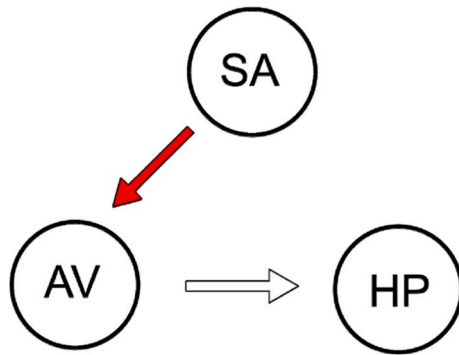


Fig. 7. Conceptual model with SA-AV random coupling.

$$x_i^t = x_i - \tau \left( \frac{x_{i+1} - x_i}{h} \right) \quad (4)$$

The time-delayed states dependence requires an appropriate approach for calculating the Lyapunov exponents (Ferreira et al., 2014). The system can be approximated by a system of ODEs of infinite dimensions (Sprott, 2007), allowing to use the algorithm due to Wolf et al. (1985) to estimate Lyapunov exponents.

### 3. Heart rhythm

Numerical simulations of the cardiac system model are performed with the objective of presenting different system behaviors. In all simulations the following parameters are used:  $\beta_0 = 1$  mV,  $\beta_1 = 0.06$  mV,  $\beta_2 = 0.1$  mV,  $\beta_3 = 0.3$ mV. A convergence analysis reveals that time steps smaller than  $10^{-3}$  presents error of the order of  $10^{-6}$ , considered satisfactory. The following initial conditions are applied for all simulations (Gois and Savi, 2009):

$$x_0 = \left[ -0.1 \quad 0.025 \quad -0.6 \quad 0.1 \quad -3.3 \quad 2/3 \right]^T \quad (5)$$

Normal heart rhythm has unidirectional couplings in such a way that the electrical impulse is conducted from SA node to AV node and then, from AV node to HP complex. The conceptual model of this normal

behavior is schematically represented in Fig. 2. Table 1 presents the system parameters related to this conceptual model, vanishing all other parameters that are not presented. This means that the system does not present external stimuli:  $\rho_{SA} = \rho_{AV} = \rho_{HP} = \omega_{SA} = \omega_{AV} = \omega_{HP} = 0$ . Moreover, only the couplings  $k_{SA-AV}$ ,  $k_{AV-HP}$ ,  $k_{SA-AV}^c$  and the following time delay  $\tau_{SA-AV}$ ,  $\tau_{SA-AV}$  do not vanish.

Fig. 3 presents the simulated normal ECG and each oscillator response that compose ECG response. This ECG captures the main features of the experimental ECG, presenting P, QRS and T waves. State spaces are presented in Fig. 4 considering different subspaces:  $\{X, \dot{X}\}$ ,  $\{x_1, x_2\}$ ,  $\{x_3, x_4\}$  and  $\{x_5, x_6\}$ . A first analysis reveals closed curves that would be associated with periodic behavior. Nevertheless, Lyapunov exponents estimation, excluding the exponent associated with time, points to null values that characterize quasi-periodic response.

Fig. 5 presents a histogram of the R-R interval of the normal rhythm showing a mean  $\mu = 6.403$ , and standard deviation,  $\sigma = 0.001$ . This mean value can be employed to define a stroboscopic view of the system dynamics, building a Poincaré section with this reference period.

### 3.1. Pathological rhythms

The ability of the proposed model to describe pathological rhythms is an essential point to be considered in order to establish a connection between dynamics and physiology. This can be useful to establish different clinical strategies. In addition, the use of mathematical models is an interesting possibility to be employed on artificial pacemakers. Based on these argues, dynamical comprehension is an essential point that needs to be explored.

In this regard, some pathological responses are simulated by changing model parameters. Fig. 6 presents a general comparison between numerical and experimental data of heart rhythms including normal and pathological ones. Parameters for these results are presented in Table 2, considering that the ones that are not presented are equal to normal case presented in Table 1. It should be highlighted that model can capture the general behavior of all ECGs. Besides, results have a stationary nature and therefore.

The idea that heart rhythms have a stationary nature motivate some reflections about pathologies. The emerging of pathologies needs to be related to some parameter change, which makes sense especially considering external stimulus. Nevertheless, it is possible to imagine some different evolution due to random reasons. The next section introduces the idea of random connections that can explain the evolution of pathologies from a normal rhythm.

### 4. Random effects

This section deals with random effects establishing the coupling among the oscillators that represent cardiac pacemakers. Nondeterministic effects are treated considering that oscillator couplings are random variables. Therefore, coupling parameters are treated as normal distributions around a nominal value represented by the mean with standard deviations. Based on that, coupling terms can be written as follows,

$$k_i \sim N(\bar{k}_i, \sigma_k^2) \quad (6)$$

where  $\bar{k}_i$  is the mean, nominal value, and  $\sigma_k$  is the standard deviation of the normal distribution.

It is important to highlight the difference between mean and standard deviation of the coupling distribution ( $\bar{k}_i$  and  $\sigma_k$ ) and the mean and standard deviation on R-R interval histograms ( $\mu$  and  $\sigma$ ), discussed in the previous section.

Basically, four different situations are considered: SA-AV coupling, AV-SA coupling, AV-HP coupling and HP-AV coupling. The following sections present the analysis of these situations, showing the pathological behaviors that evolve from normal rhythm.

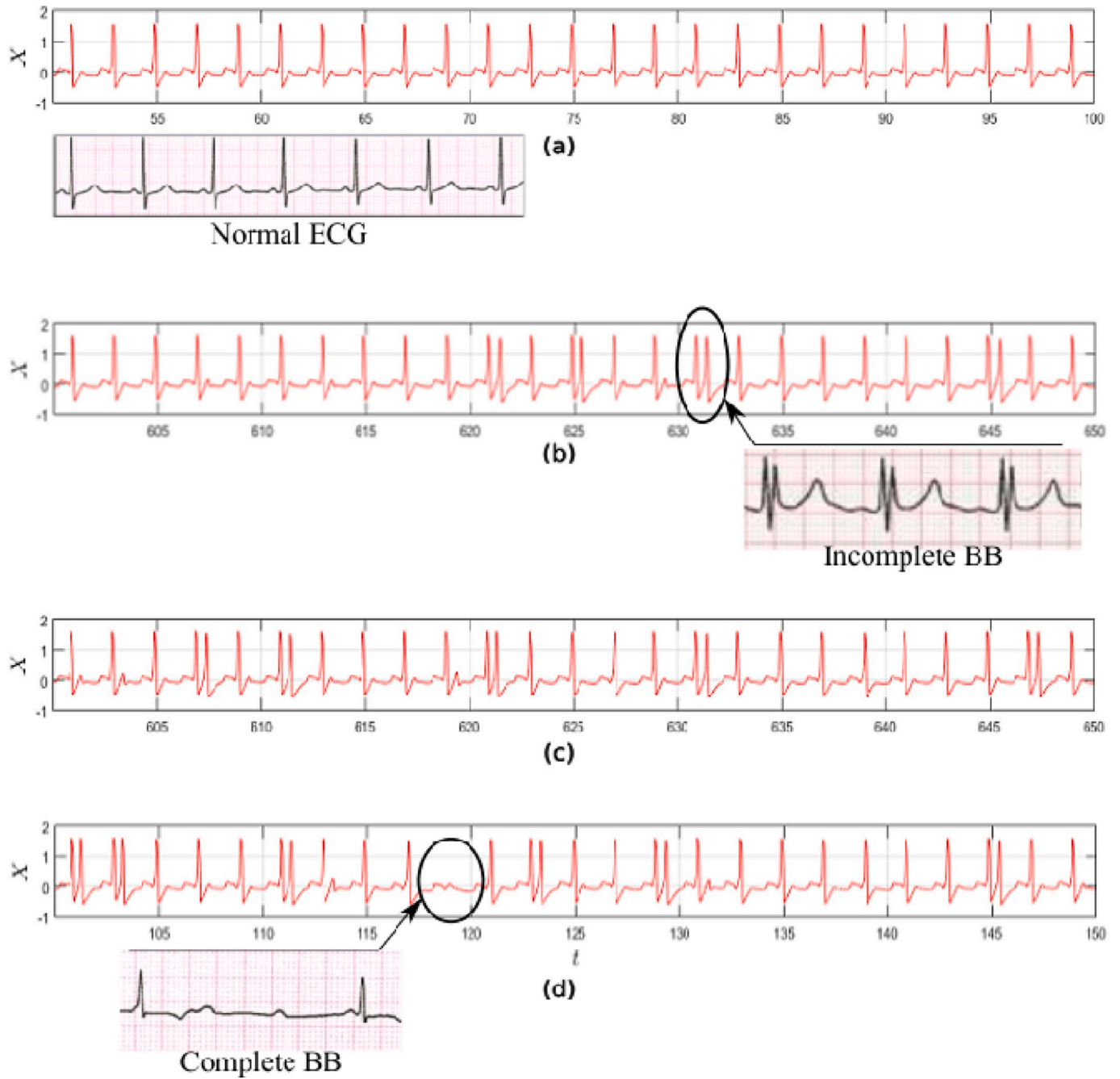


Fig. 8. Random SA-AV coupling ECGs highlighting experimental data. (a)  $\sigma_k = 0.5$ ; (b)  $\sigma_k = 1.5$ ; (c)  $\sigma_k = 2.5$ ; (d)  $\sigma_k = 3.5$ .

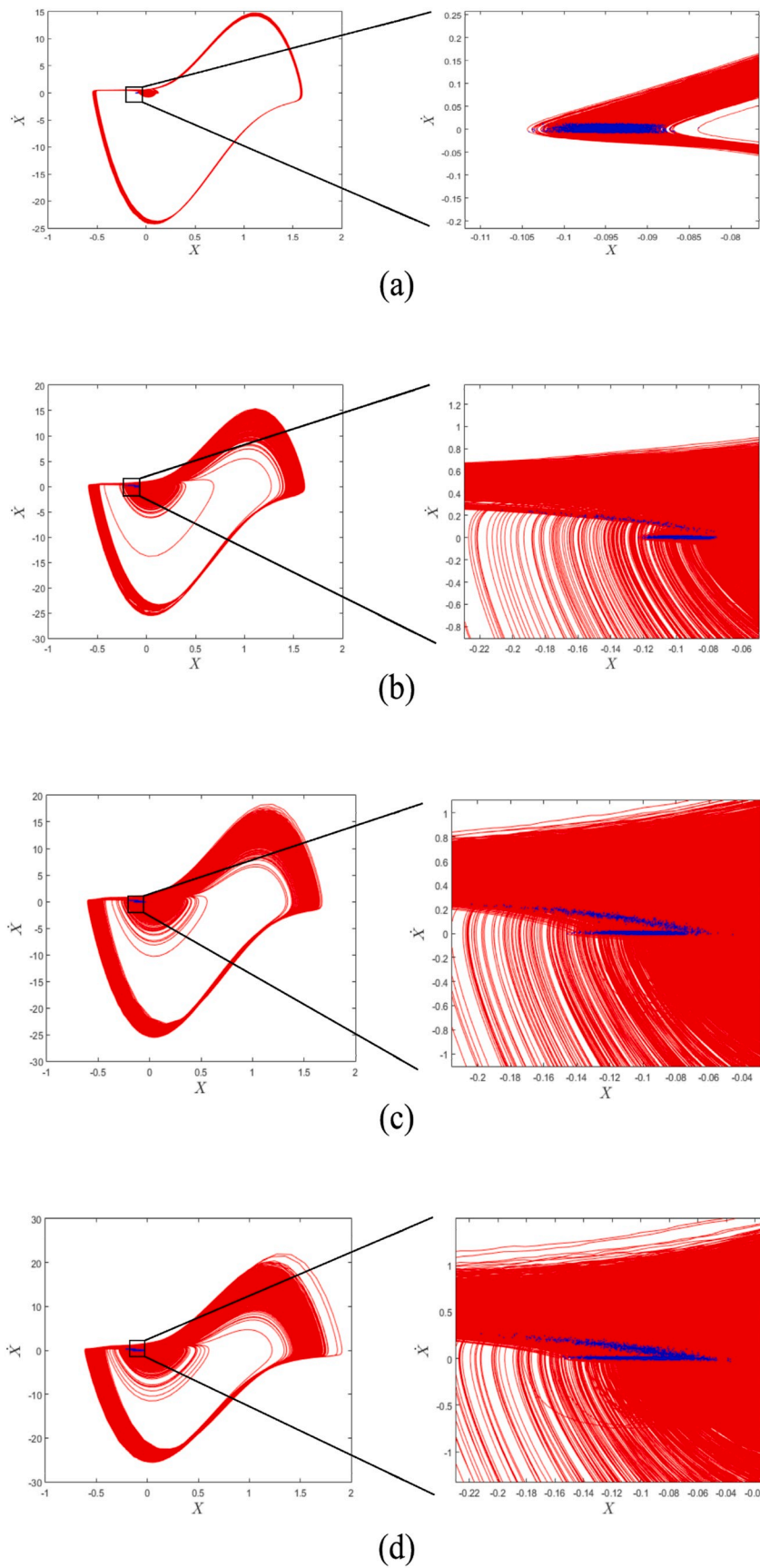


Fig. 9. Random SA-AV coupling state spaces and Poincaré maps. (a)  $\sigma_k = 0.5$ ; (b)  $\sigma_k = 1.5$ ; (c)  $\sigma_k = 2.5$ ; (d)  $\sigma_k = 3.5$ .

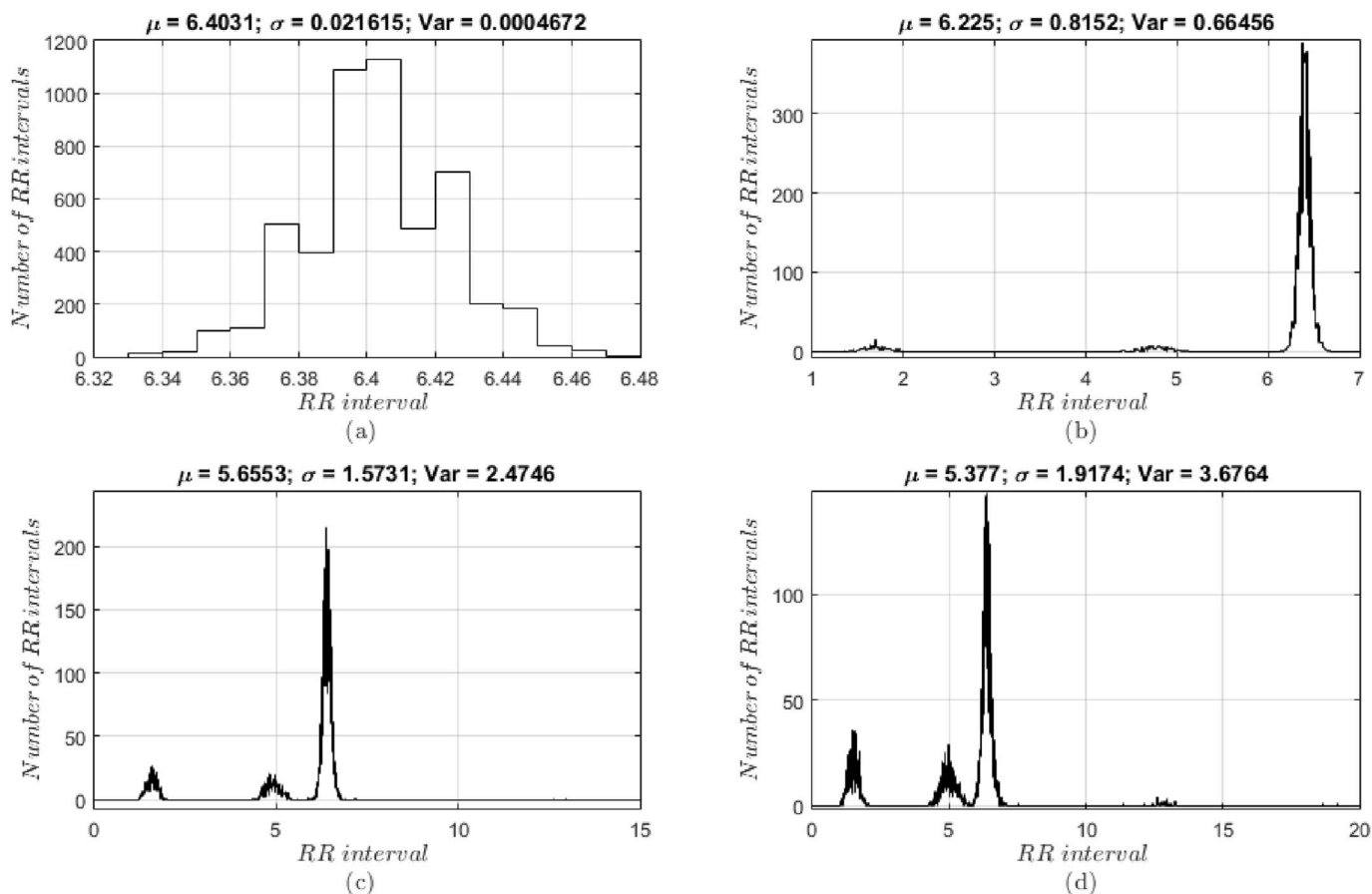


Fig. 10. SA-AV random coupling R-R histograms. (a)  $\sigma_k = 0.5$ ; (b)  $\sigma_k = 1.5$ ; (c)  $\sigma_k = 2.5$ ; (d)  $\sigma_k = 3.5$ .

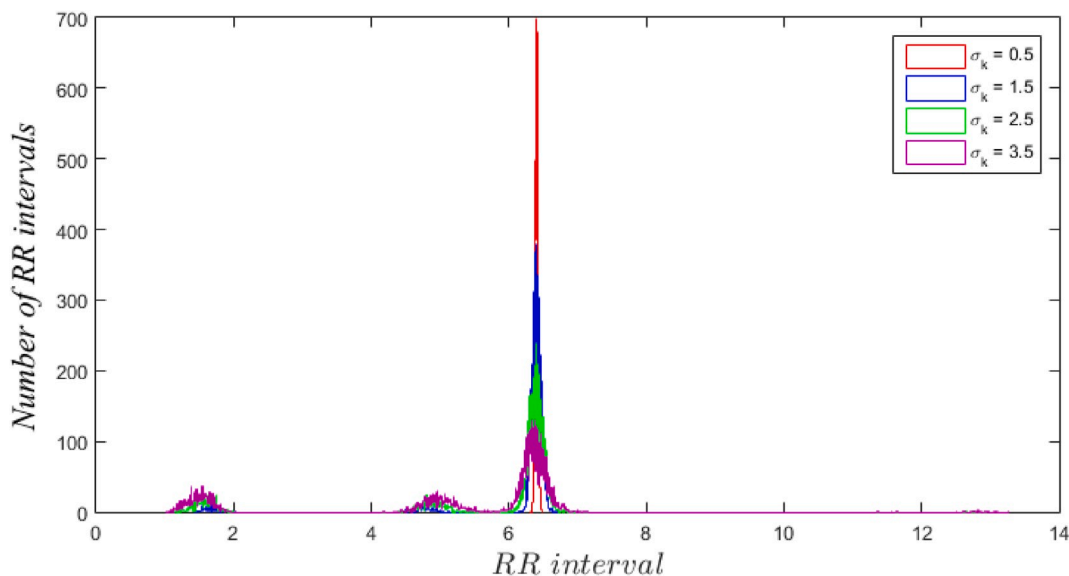


Fig. 11. SA-AV random coupling: comparison of R-R histograms for different standard deviations.

#### 4.1. Random SA-AV coupling

Consider the SA-AV coupling represented by the parameter  $k_{SA-AV} \sim N(\bar{k}_{SA-AV}, \sigma_k^2)$ . Normal heart function has a nominal value  $\bar{k}_{SA-AV} = 3$ . Fig. 7 identifies the couplings, highlighting the random coupling. Results for different values of standard deviation,  $\sigma_k$ , are presented in

Fig. 8 showing ECGs. It is noticeable that the increase of  $\sigma_k$  induces incomplete and complete Branch Blocks (BB) (Canabrava, 2014) changing the ECG characteristic. Incomplete BB is characterized by QRS complex with double R peaks. On the other hand, complete BB is characterized by the absence of QRS complex. Experimental data depicted in Fig. 8 highlights the pathological characteristics induced by the random coupling. ECG state spaces and Poincaré maps are presented in Fig. 9

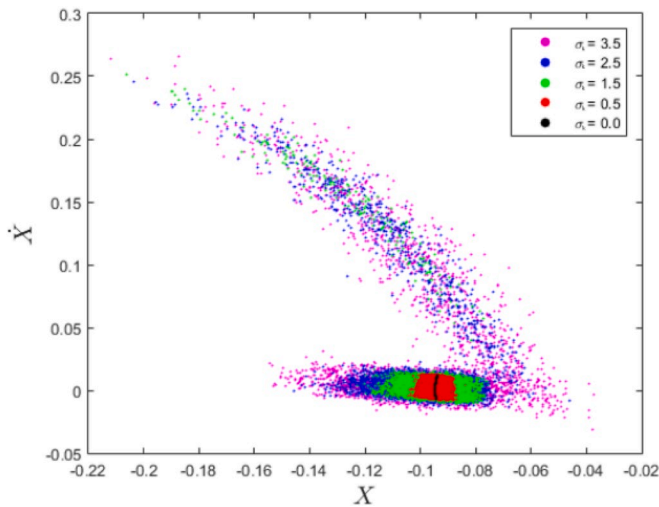


Fig. 12. SA-AV random coupling: Poincaré maps for different standard deviations.

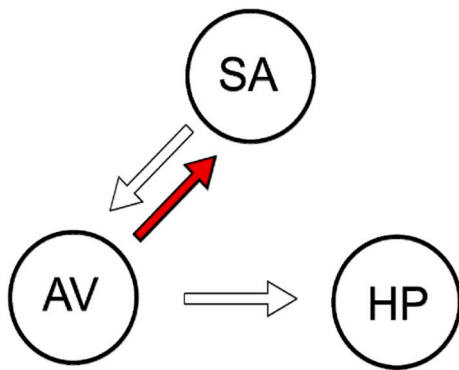


Fig. 13. Conceptual model of the AV-SA random coupling.

showing that the increase of  $\sigma_k$  causes the spreading of orbits around the normal orbit and also the increase of Poincaré map space portion.

R-R interval histograms are shown in Fig. 10 for each one of the different standard deviations. When  $\sigma_k = 0.5$ , the RR is close to the deterministic case. When  $\sigma_k = 1.5$ , peaks appear below the reference R-R, which may be related to incomplete Branch Block (Canabrava, 2014), where the QRS complex has double R peaks. For values greater than  $\sigma_k = 2.5$ , response reaches a complete Branch Block (absence of QRS complex), which is characterized by the appearance of peaks to the right of the histogram, corresponding to R-R values greater than  $\mu$ .

Figs. 11 and 12 show comparisons of the R-R histograms and Poincaré maps for the treated cases. The trend of decreasing the mean  $\mu$  of the R-R intervals with the increase of  $\sigma_k$  shows a correlation between the variability of the parameter  $k_{SA-AV}$  and the Branch Block. Poincaré Maps of the normal ECG is represented by a line (black) and the increase of  $\sigma_k$  tends to evolve to a cloud around this line (red region). For  $\sigma_k = 1.5$ , when incomplete BB appears, Poincaré section changes its shape presenting a curved cloud (green and blue regions), which is spread from the initial cloud. When  $\sigma_k = 3.5$ , complete BB occurs and it is possible to observe a spreading of the initial cloud (purple).

#### 4.2. Random AV-SA coupling

Random variations of the coupling AV-SA are now in focus considering the conceptual model presented in Fig. 13. This coupling is represented by the parameter  $k_{AV-SA} \sim N(\bar{k}_{AV-SA}, \sigma_k^2)$ , where the normal

ECG has a nominal value  $\bar{k}_{AV-SA} = 0$ .

ECGs for different values of standard deviations are presented in Fig. 14. Note that the increase of  $\sigma_k$  is related to an increase of R-R irregularity. This behavior is physiologically related to atrial fibrillation where irregular contractions in atria, caused by multiple electrical foci, are reflected on irregularities of the R-R interval. Experimental data presented in Fig. 14 illustrate these changes. ECG state spaces and Poincaré maps are presented in Fig. 15 showing that for  $\sigma_k < 0.5$  (Fig. 15-a, b), which time series response are apparently normal, there is significant changes in state spaces and Poincaré sections. For greater values of  $\sigma_k$ , incomplete and complete BB (Fig. 15-c, d) are related to analogous behaviors of the previous sections, but covering a larger area. The occurrence of atrial fibrillation (Fig. 15-e) is related to denser state spaces and Poincaré sections.

R-R interval histograms are shown in Fig. 16. Note that for  $\sigma_k > 2.0$ , R-R values are distributed over a larger range than the previous case, which is reflected on the considerable increase of R-R standard deviation. This spread of histogram values with Poincaré map patterns is an indication that the response presents chaotic characteristics.

Figs. 17 and 18 provide comparisons of the R-R histograms and the Poincaré maps. In this case, it is reasonable to think of a possible relation between the variability  $k_{AV-SA}$  and atrial fibrillation. In addition, it is observed that Poincaré maps occupy a region greater than the ones related to normal rhythm, which can be used as a diagnostic tool. In this case, the increase of  $\sigma_k$  is related to an evolution of histograms and Poincaré sections with characteristics explained earlier for incomplete and complete BB but also with characteristics related to atrial fibrillation (larger range in histograms and area of the Poincaré sections).

#### 4.3. Random AV-HP coupling

Random AV-HP coupling is now of concern considering coupling parameter as  $k_{AV-HP} \sim N(\bar{k}_{AV-HP}, \sigma_k^2)$  with nominal value  $\bar{k}_{AV-HP} = 55$ . Fig. 19 presents the conceptual model.

Fig. 20 shows the ECG considering different standard deviations,  $\sigma_k$ . For  $\sigma_k < 55.0$ , ECG does not have significant differences when compared to the normal one. Nevertheless, the increase of standard deviations tends to alter the ECG in a dramatic way. This behavior indicates a ventricular tachycardia (Dubin, 1996) where sequential R-peaks appear or QRS complex becomes greater due to irregular functioning of ventricles. Once again, experimental data confirm the changes helping their visualization.

Fig. 21 shows ECG state spaces and Poincaré maps. Even for imperceptible changes in time series (for  $\sigma_k < 55.0$ ), it is possible to see significant changes in state space (Fig. 21-a, b, c). One can also observe characteristic changes of state space and Poincaré sections due to incomplete BB (Fig. 21-d,e,f). It should be highlighted that the enlargement around the bigger loop of state space can be related to ventricular tachycardia, indicating a trend.

(a)  $\sigma_k = 1.0$ ; (b)  $\sigma_k = 5.0$ ; (c)  $\sigma_k = 30.0$ ; (d)  $\sigma_k = 55.0$ ; (e)  $\sigma_k = 110.0$ ; (f)  $\sigma_k = 220.0$ ; (g)  $\sigma_k = 440.0$ .

R-R histograms are presented in Fig. 22 where it is possible to observe a trend of decreasing the mean  $\mu$  with the increase of  $\sigma_k$ . The occurrence of peaks smaller than the reference mean ( $\mu = 6.403$ ) represents that R waves are becoming closer, which means that heart frequency is increasing, a behavior related to a ventricular tachycardia (Dubin, 1996).

A comparison among R-R histograms is presented in Fig. 23. Note that peaks appear on left side of histogram reflecting the R-R interval reduction caused by closer and closer R peaks. Poincaré maps comparison is presented in Fig. 24. Once again, the increase of  $\sigma_k$  causes the Poincaré map spreading to a different pattern from previous cases. Incomplete BB response causes expansion of a cloud around normal Poincaré section, while ventricular tachycardia trends to stretch section to the left. This can be used to identify and classify different responses.

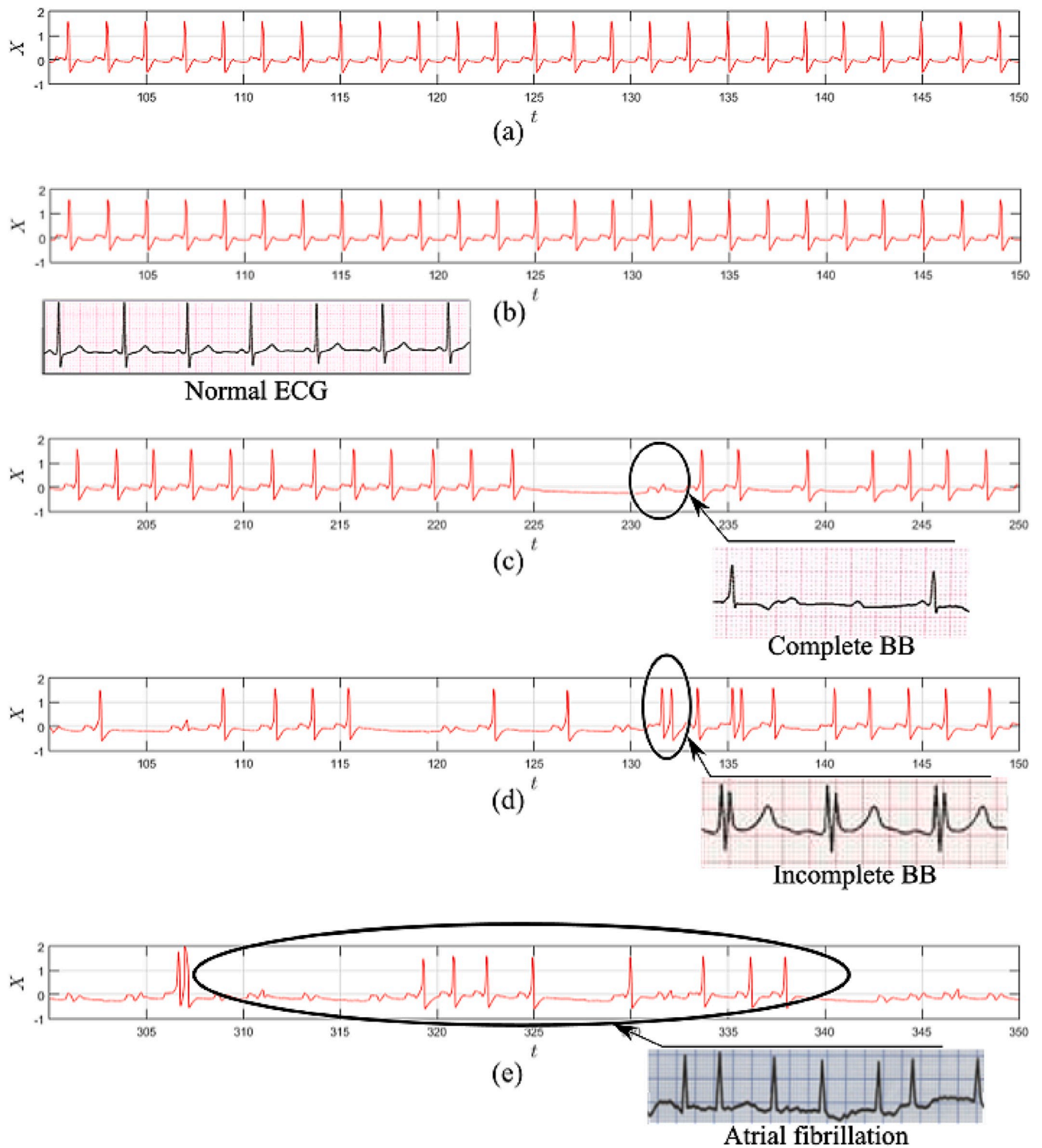


Fig. 14. AV-SA random coupling ECG highlighting experimental data. (a)  $\sigma_k = 0.1$ ; (b)  $\sigma_k = 0.5$ ; (c)  $\sigma_k = 2.0$ ; (d)  $\sigma_k = 6.0$ ; (e)  $\sigma_k = 14.0$ .

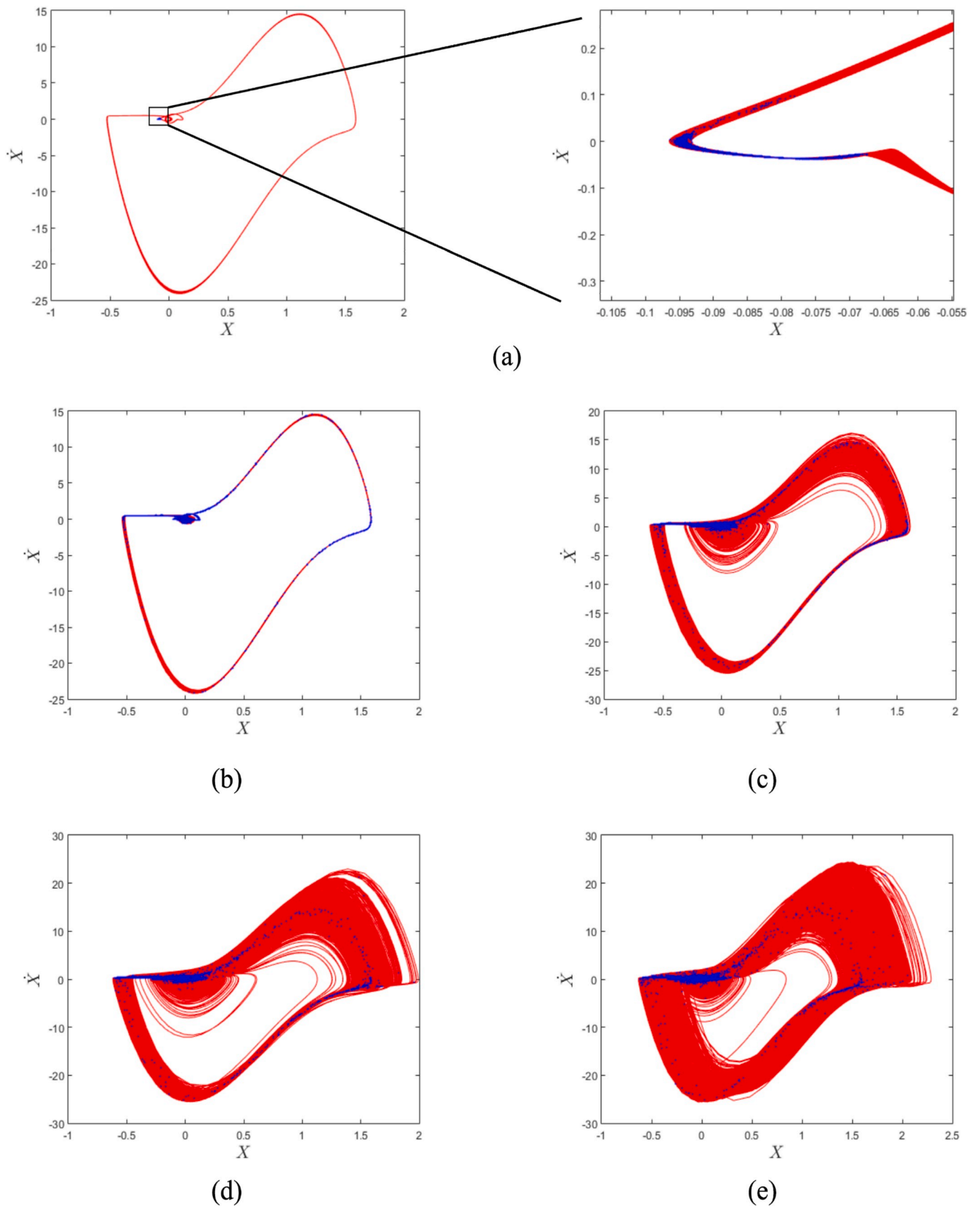


Fig. 15. AV-SA random coupling state spaces and Poincaré maps. (a)  $\sigma_k = 0.1$ ; (b)  $\sigma_k = 0.5$ ; (c)  $\sigma_k = 2.0$ ; (d)  $\sigma_k = 6.0$ ; (e)  $\sigma_k = 14.0$ .

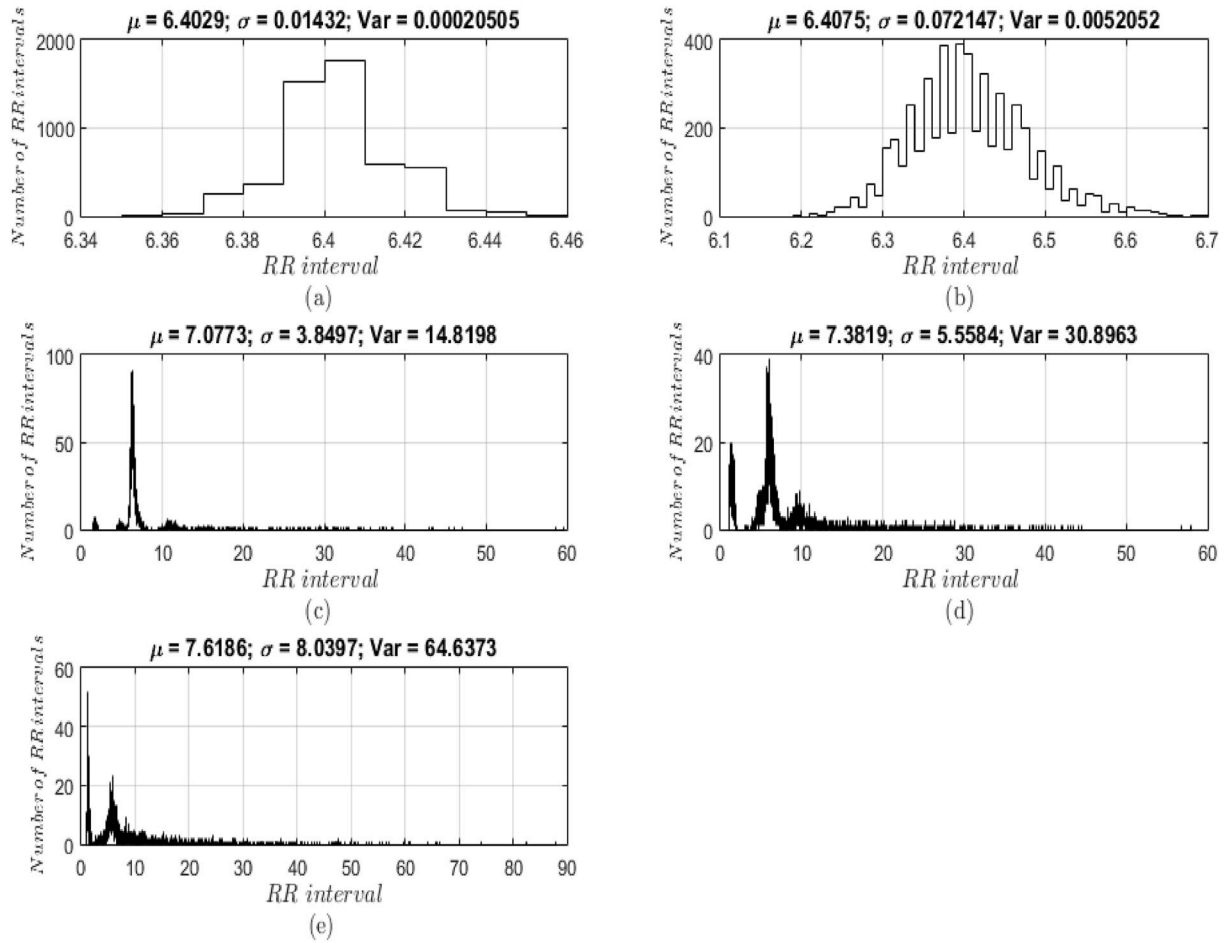


Fig. 16. AV-SA random coupling R-R histograms. (a)  $\sigma_k = 0.1$ ; (b)  $\sigma_k = 0.5$ ; (c)  $\sigma_k = 2.0$ ; (d)  $\sigma_k = 6.0$ ; (e)  $\sigma_k = 14.0$ .

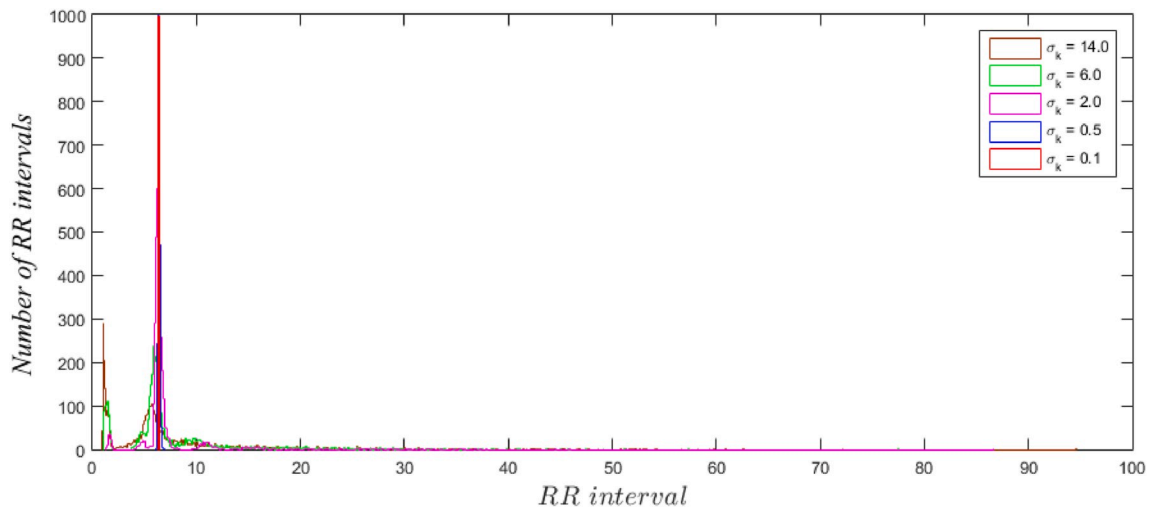


Fig. 17. AV-SA random coupling: comparison of R-R histograms for different standard deviations.

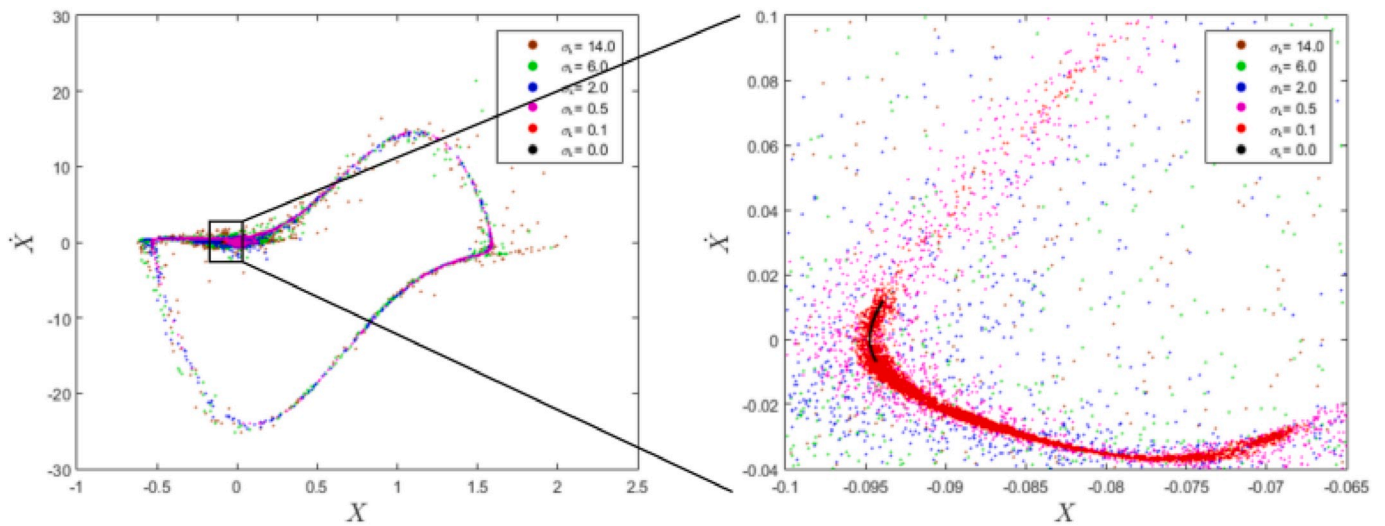


Fig. 18. AV-SA random coupling: Poincaré maps for different standard deviations.

4.4. Random HP-AV coupling

Random HP-AV coupling is now in focus considering  $k_{HP-AV} \sim N(\bar{k}_{HP-AV}, \sigma_k^2)$  where nominal value is  $\bar{k}_{HP-AV} = 0$ . Conceptual model is presented in Fig. 25 represents.

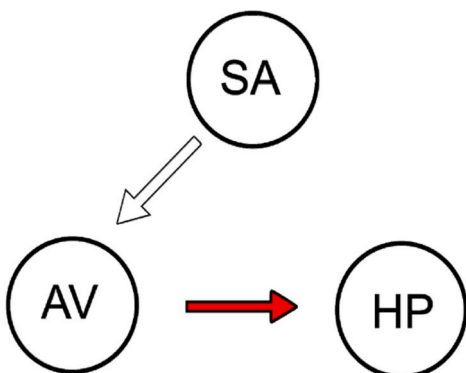


Fig. 19. Conceptual model for AV-HP coupling.

ECGs are presented in Fig. 26 showing that the increase of  $\sigma_k$  tends to induce the occurrence of R waves sequences, characteristic of ventricular flutter. For values greater than  $\sigma_k = 20$ , typical changes of Branch Block appear (absence of R waves). All these variations are confirmed by experimental data depicted in the Figure. Fig. 27 shows state spaces and Poincaré maps that give a different visualization of the involved rhythms. Accompanied by changes caused by incomplete BB (Fig. 27-a, b, c, d), already explained, the enlargement of greater loop can be related to ventricular flutter (Fig. 27-e, f).

Fig. 28 shows R-R interval histograms. In this case, a decrease in the mean  $\mu$  is observed as  $\sigma_k$  increases (sequential R waves). When  $\sigma_k = 30$ , there is an increase of the mean value, related to the absence of R waves. A comparative analysis of R-R histograms (Fig. 29) and Poincaré maps (Fig. 30) shows different shapes of R-R peaks and different shapes of Poincaré maps from the other studied cases. Once again, it helps to identify responses and pathologies. As  $\sigma_k$  increases, Poincaré section evolves to a stretched cloud, which is associated with incomplete BB. This cloud around greater loop is related to ventricular flutter behavior indicating a trend to this pathology.

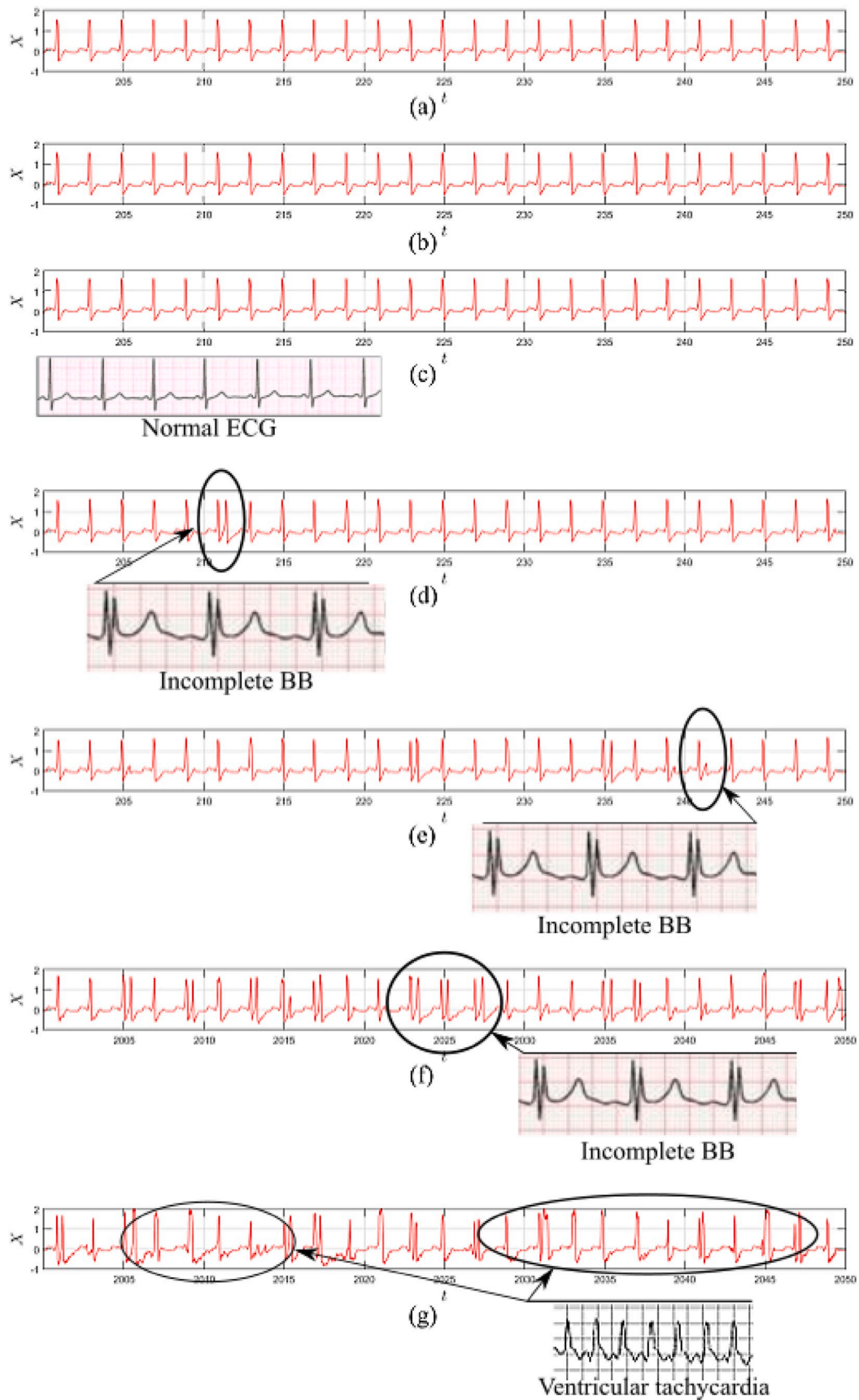


Fig. 20. AV-HP random coupling ECG highlighting experimental data.

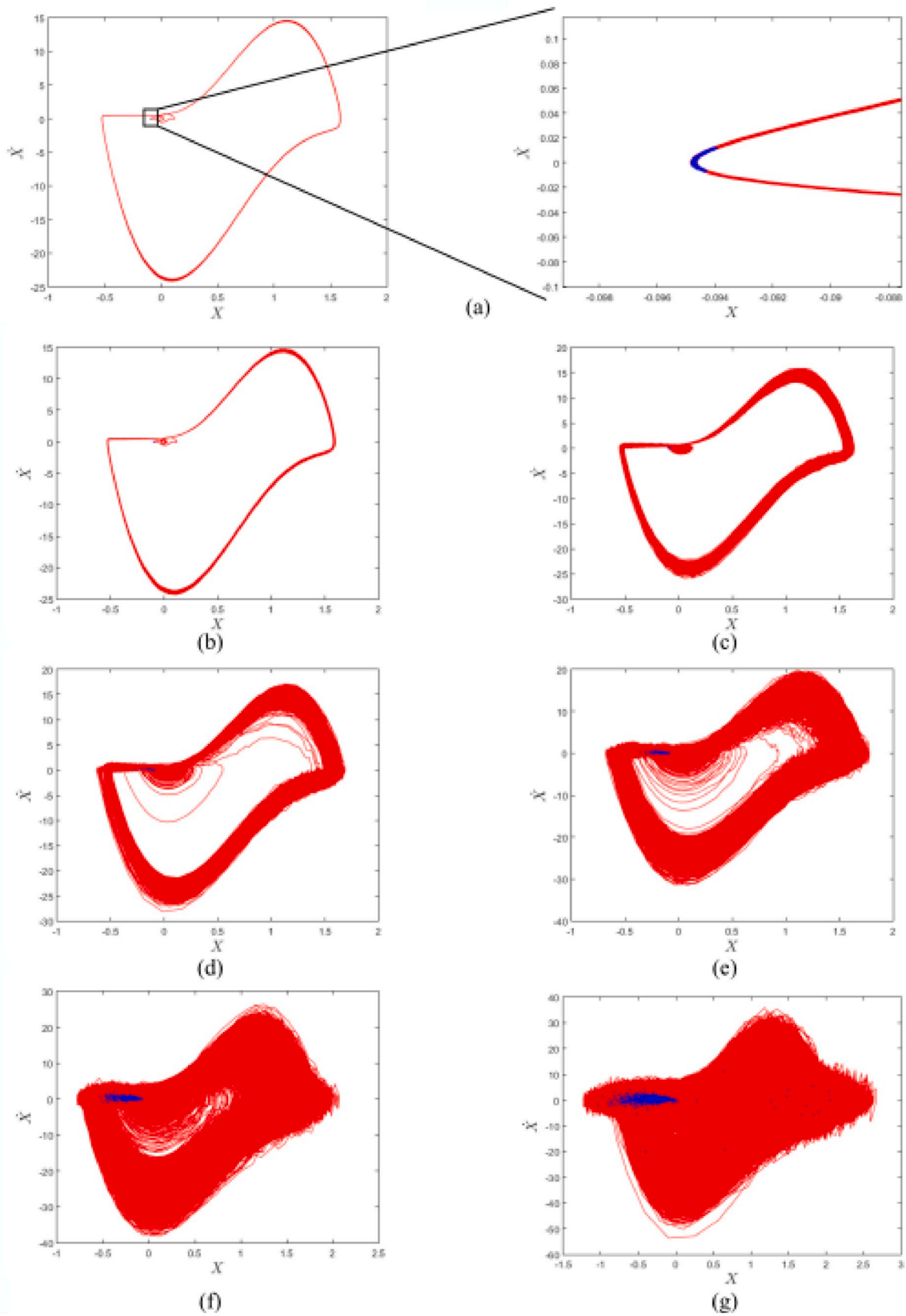


Fig. 21. AV-HP random coupling state spaces and Poincaré maps. (a)  $\sigma_k = 1.0$ ; (b)  $\sigma_k = 5.0$ ; (c)  $\sigma_k = 30.0$ ; (d)  $\sigma_k = 55.0$ ; (e)  $\sigma_k = 110.0$ ; (f)  $\sigma_k = 220.0$ ; (g)  $\sigma_k = 440.0$ .

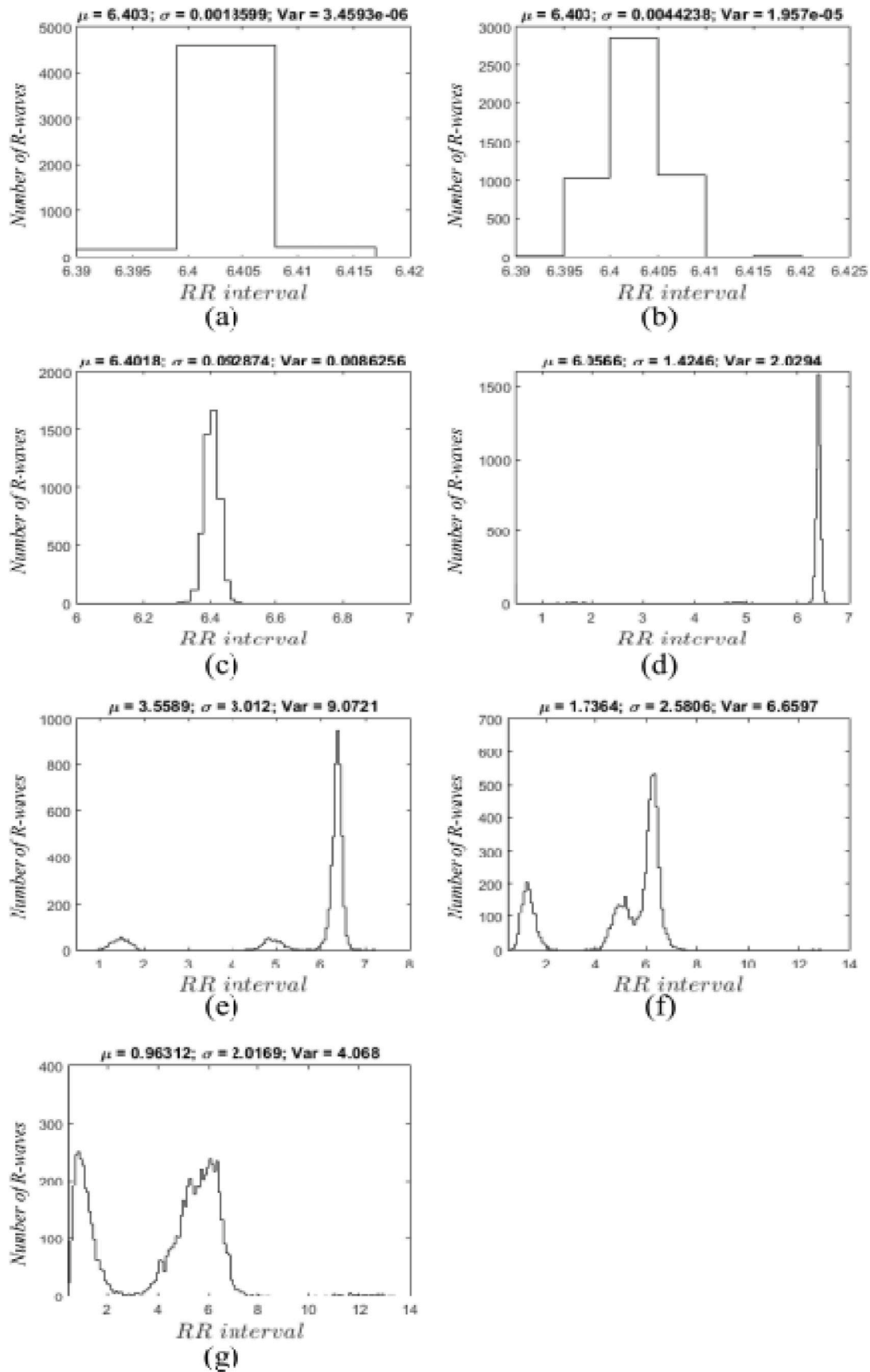


Fig. 22. AV-HP random coupling R-R histograms. (a)  $\sigma_k = 1.0$ ; (b)  $\sigma_k = 5.0$ ; (c)  $\sigma_k = 30.0$ ; (d)  $\sigma_k = 55.0$ ; (e)  $\sigma_k = 110.0$ ; (f)  $\sigma_k = 220.0$ ; (g)  $\sigma_k = 440.0$ .

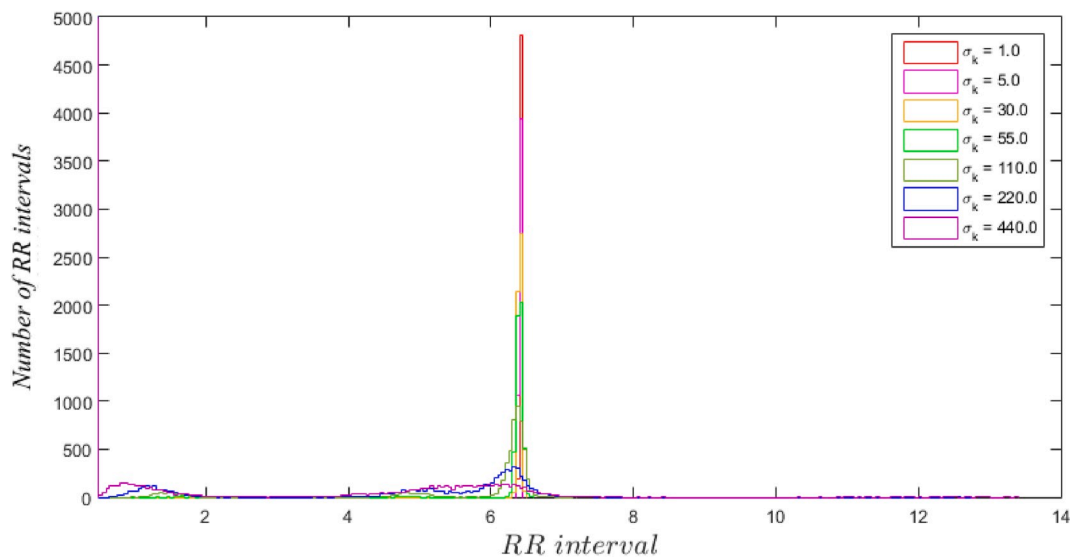


Fig. 23. AV-HP random coupling: comparison of R-R histograms for different standard deviations.

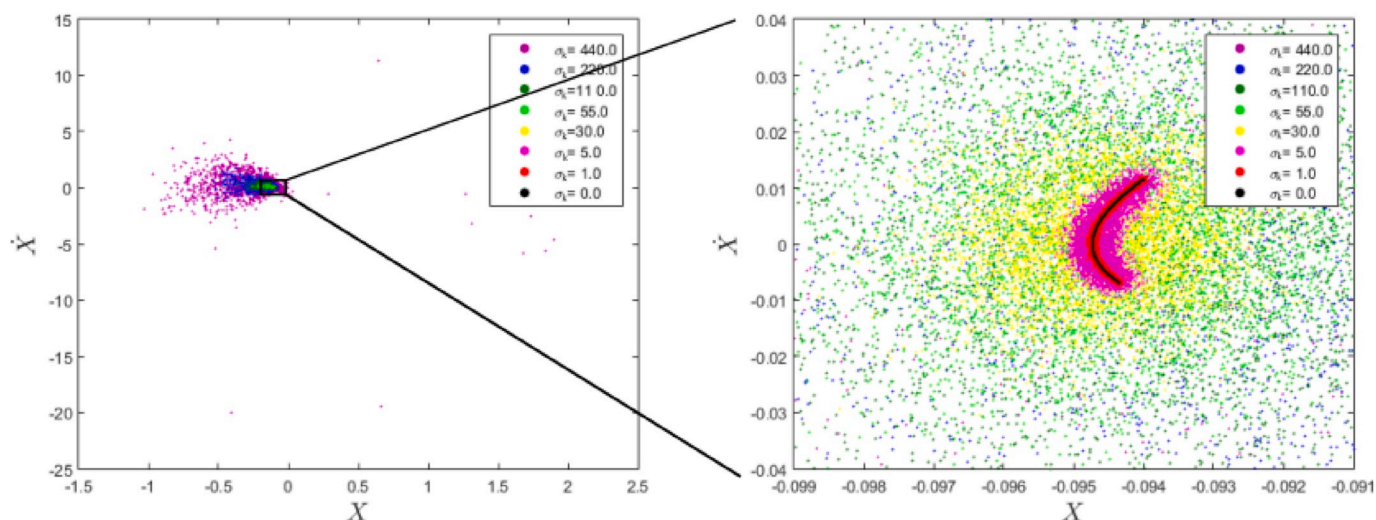


Fig. 24. AV-HP random coupling: Poincaré maps for different standard deviations.

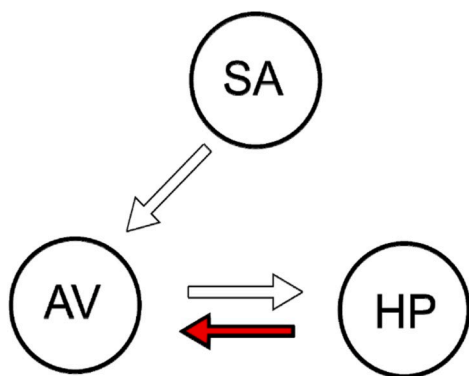


Fig. 25. Conceptual model for HP-AV random coupling.

5. Conclusion

Cardiac rhythms are investigated using a nonlinear and nondeterministic perspective showing that these effects can be combined to

represent natural system richness. A mathematical model composed by three-coupled oscillators with time-delayed couplings is employed to represent cardiac rhythms. This model reproduces ECGs for various situations of heart functioning, being able to capture either normal or pathological rhythms. The effects of randomness on the system response are investigated by considering random couplings. Basically, pathological behaviors can evolve from normal rhythms due to random couplings. In light of this investigation, it is concluded that cardiac system model has great potential to assist rich heart dynamics comprehension, being useful for disease diagnosis. Nonlinear dynamics analysis have proved to be useful for a proper comprehension of the heart physiology since it highlights response variations that are imperceptible on time series. Considering state space characteristics, it is noticeable that normal rhythm presents a closed curve with two loops while pathological rhythms tend to be characterized by an open trajectory with denser orbits around the normal one. Poincaré map presents normal response characterized by a line and, on the other hand, pathological responses exhibit clouds of points around the normal one. It is noticeable that Poincaré map evolves to different shapes that can be used to identify and predict different pathologies.

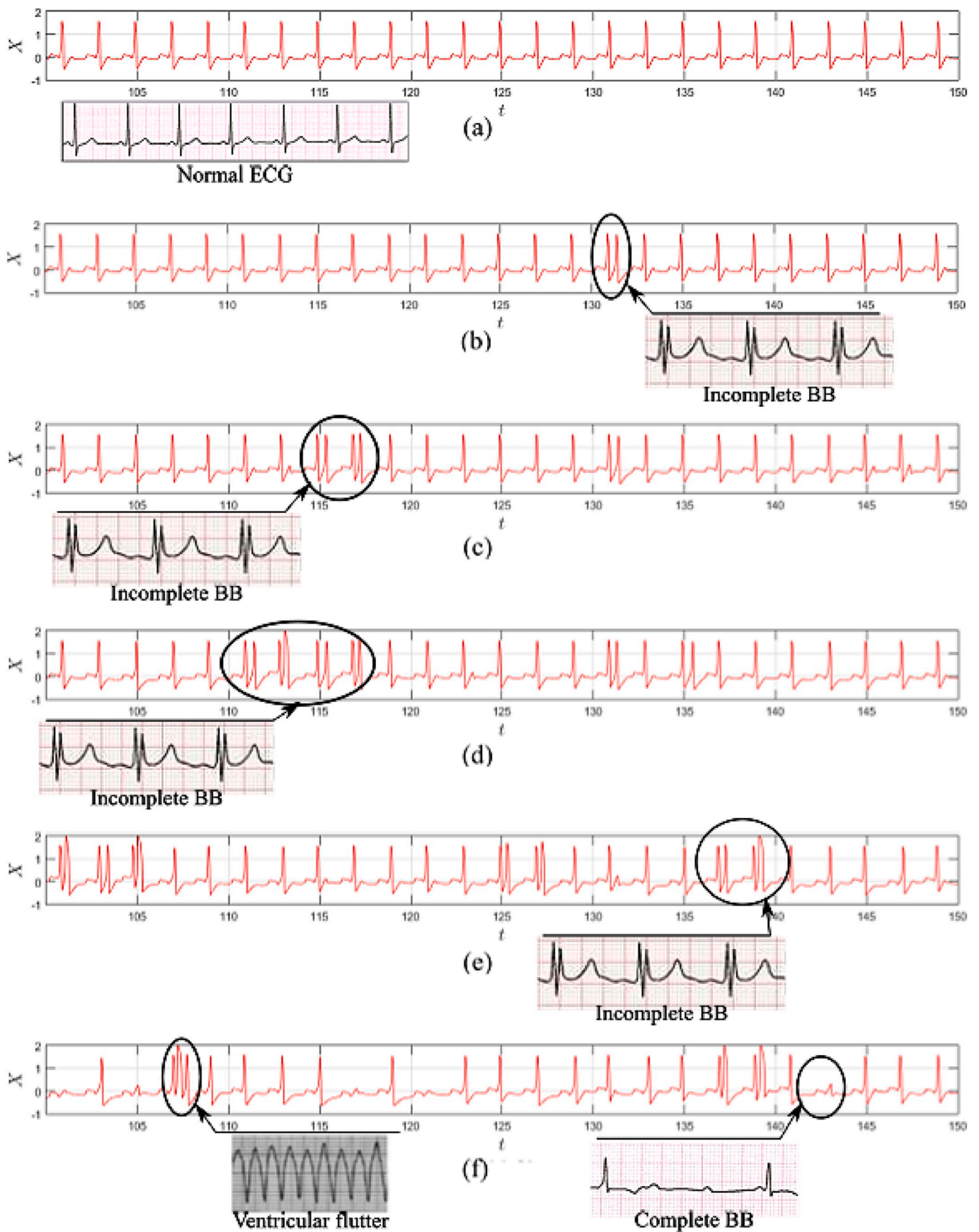


Fig. 26. HP-AV random coupling ECG highlighting experimental data. (a)  $\sigma_k = 1.0$ ; (b)  $\sigma_k = 3.0$ ; (c)  $\sigma_k = 5.0$ ; (d)  $\sigma_k = 10.0$ ; (e)  $\sigma_k = 20.0$ ; (f)  $\sigma_k = 30.0$ .

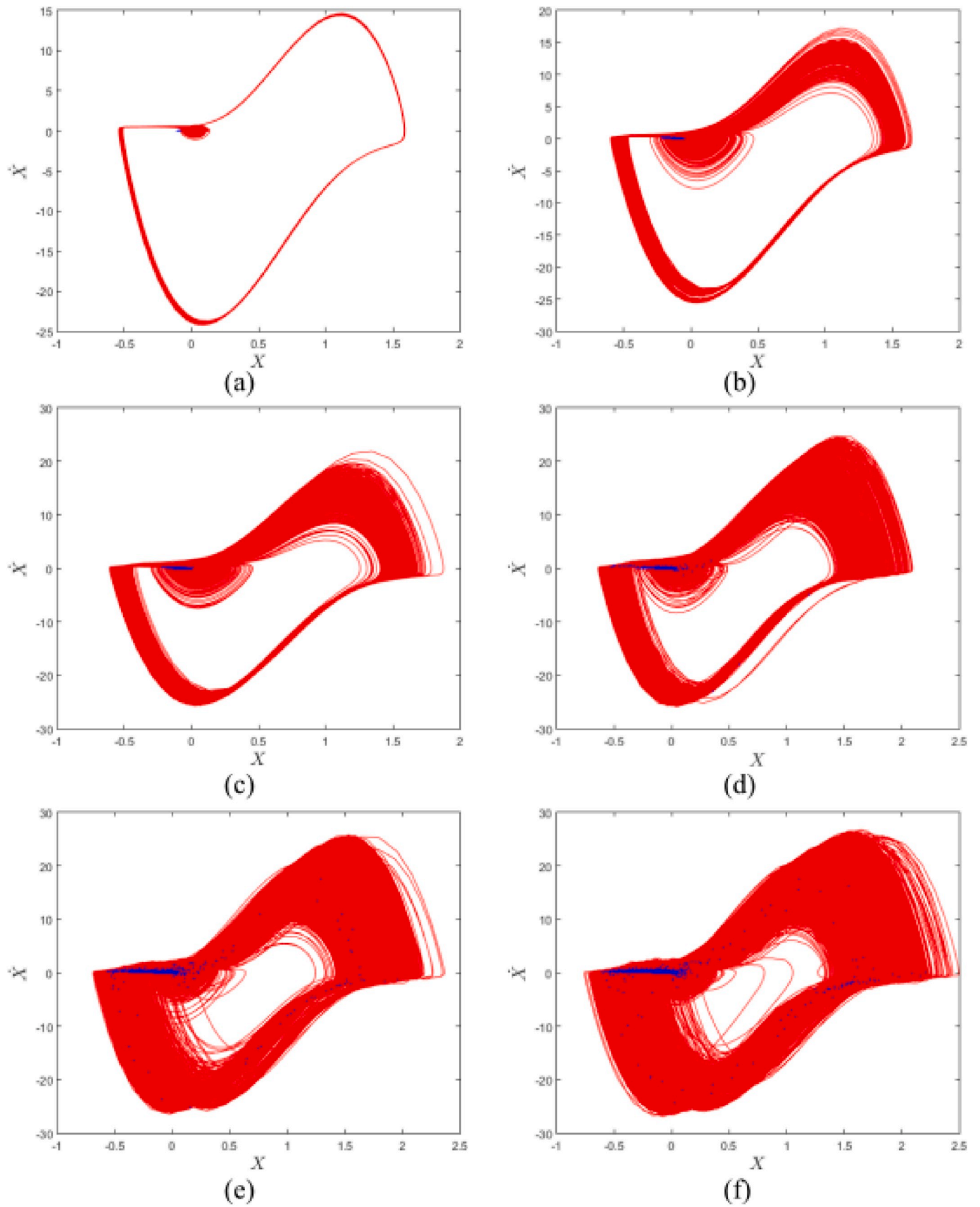


Fig. 27. HP-AV random coupling state spaces and Poincaré maps. (a)  $\sigma_k = 1.0$ ; (b)  $\sigma_k = 3.0$ ; (c)  $\sigma_k = 5.0$ ; (d)  $\sigma_k = 10.0$ ; (e)  $\sigma_k = 20.0$ ; (f)  $\sigma_k = 30.0$ .

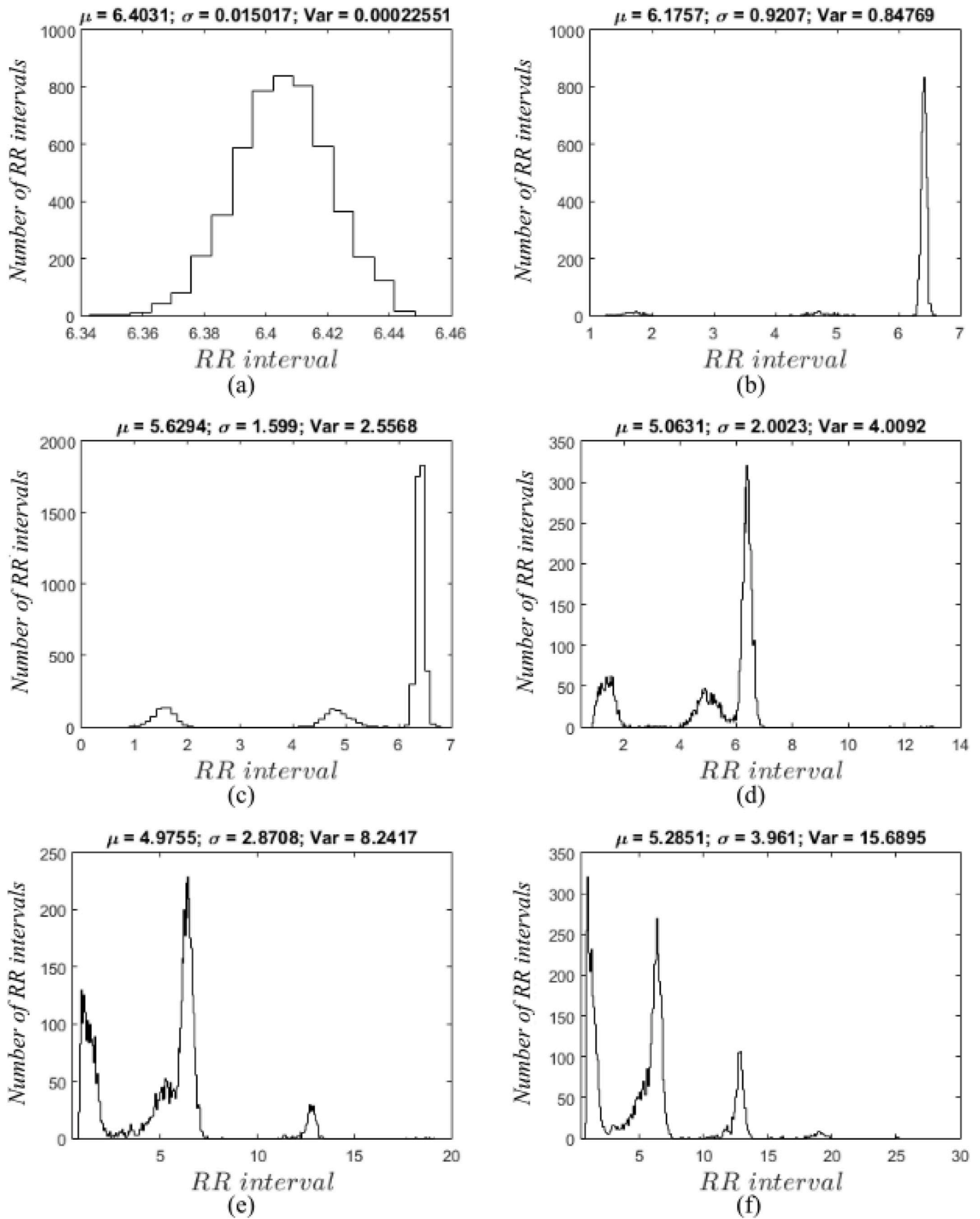


Fig. 28. HP-AV random coupling R-R histograms. (a)  $\sigma_k = 1.0$ ; (b)  $\sigma_k = 3.0$ ; (c)  $\sigma_k = 5.0$ ; (d)  $\sigma_k = 10.0$ ; (e)  $\sigma_k = 20.0$ ; (f)  $\sigma_k = 30.0$ .

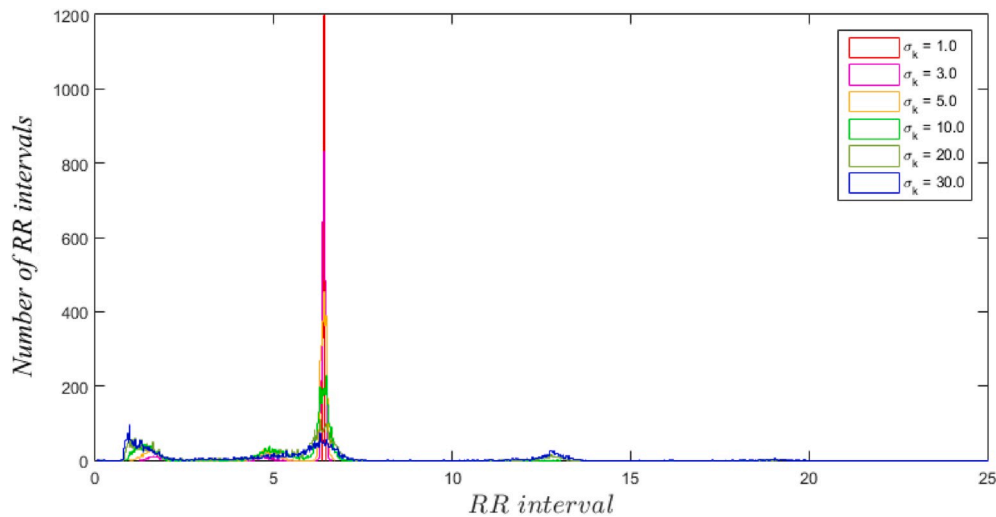


Fig. 29. HP-AV random coupling: comparison of R-R histograms for different standard deviations.

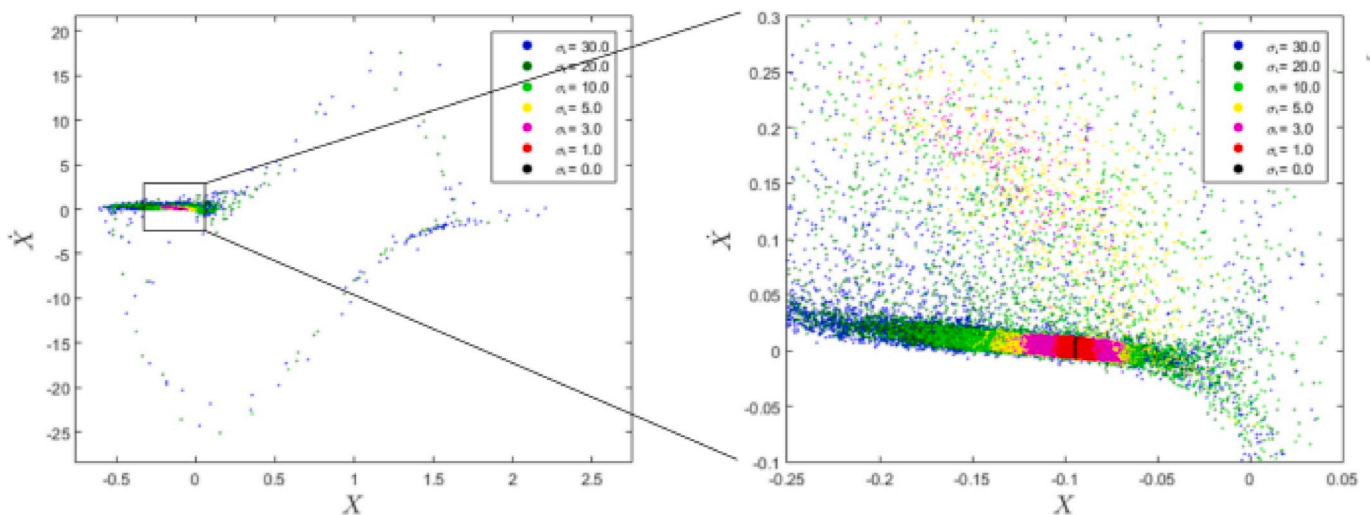


Fig. 30. HP-AV random coupling: Poincaré maps for different standard deviations.

## Declaration of competing interest

The authors declare that they have no conflict of interest.

## Acknowledgements

The authors would like to acknowledge the support of the Brazilian Research Agencies CNPq, CAPES and FAPERJ.

## References

- Aronis, K.N., Berger, R.D., Calkins, H., Chrispin, J., Marine, J.E., Spragg, D.D., Tao, S., Tandri, H., Ashikaga, H., 2018. "Is human atrial fibrillation stochastic or deterministic? – insights from missing ordinal patterns and causal entropy-complexity plane analysis" *Chaos. Interdis. J. Nonlinear. Sci.* 28 (6), 063130, 2018.
- Bozóki, Z., 1997. Chaos theory and power spectrum analysis in computerized cardiocardiography. *Eur. J. Obstet. Gynecol. Reprod. Biol.* 71 (2), 163–168.
- Buchner, T., Petelczyc, M., Zebrowski, J.J., Prejbisz, A., Kabat, M., Januszewicz, A., Szelenberger, W., 2009. "On the nature of heart rate variability in a breathing normal subject: a stochastic process analysis", *Chaos. Interdis. J. Nonlinear. Sci.* 19 (2), 028504.
- Canabrava, S., 2014. Eletrocardiografia. Med eLearning Cursos Interativos.
- Cunningham, W.J., 1954. A nonlinear differential-difference equation of growth. *Proc. Natl. Acad. Sci. Unit. States Am.* 40 (8), 708–713.
- Dubin, D., 1996. Interpretação Rápida Do ECG. Editora de Publicações Biomédicas – EPUB, Rio de Janeiro.
- Ferreira, B.B., Savi, M.A., De Paula, A.S., 2014. Chaos control applied to cardiac rhythms represented by ECG signals. *Phys. Scripta* 89, Article 105203.
- Glass, L., 2009. Introduction to controversial topics in nonlinear science: is the normal heart rate chaotic? *Chaos. Interdis. J. Nonlinear. Sci.* 19 (2), 028501.
- Gois, S.R.S.M., Savi, M.A., 2009. "An analysis of heart rhythm dynamics using a three-coupled oscillator model", *Chaos. Sol. Fract.* 41 (5), 2553–2565.
- Grudzinski, K., Zebrowski, J.J., 2004. Modeling cardiac pacemakers with relaxation oscillators. *Physica A* 336, 153–162.
- Kaplan, D.T., 1990. Simultaneous QRS detection and feature extraction using simple matched filter basis functions. *Proc. IEEE* 503–506.
- Kantz, H., Schreiber, T., 2002. *Nonlinear Time Series Analysis, Ser. 7.* Cambridge Nonlinear Science, USA.
- Kaplan, D.T., Cohen, R.J., 1990. Is fibrillation chaos? *Circ. Res.* 67 (4), 886–892.
- Malik, M., Camm, A.J., 1995. Heart Rate Variability. Armonk, NY, Futura.
- Mansier, P., Clairambault, J., Charlotte, N., Médigue, C., Vermeiren, C., Lepape, G., Carré, F., Gounaropoulou, A., Swynghebaert, B., 1996. Linear and non-linear analyses of heart rate variability: a minireview. *Cardiovasc. Res.* 31 (3), 371–379.
- Mensour, B., Longtin, A., 1998. "Power spectra and dynamical invariants for delay-differential and difference equations". *Phys. Nonlinear Phenom.* 113 (1), 1–25.
- Moody, G., Mark, R., Zoccola, A., Mantero, S., 1985. Derivation of respiratory signals from multi-lead ECGs. *Comput. Cardiol.* 12, 113–116.
- Pan, J., Tompkins, W.J., 1985. A real-time QRS detection algorithm. *IEEE Trans. Biomed. Eng. BME-32*, 220–236.
- Son, J., Du, D., Du, Y., 2019. Stochastic modeling and dynamic analysis of the cardiovascular system with rotary left ventricular assist devices. *Math. Probl Eng.* 2019.
- Sprott, J.C., 2007. A simple chaotic delay differential equation. *Phys. Lett.* 366, 397–402.
- Van Der Pol, B., Van Der Mark, J., 1928. The heartbeat considered as a relaxation oscillator and an electrical model of the heart. *Phil. Mag.* 6, 763–775.

- Wessel, N., Riedl, M., Kurths, J., 2009. "Is the normal heart rate "chaotic" due to respiration? *Chaos: Interdis. J. Nonlinear. Sci.* 19 (2), 028508.
- Wolf, A., Swift, J.B., Swinney, H.L., Vastano, J.A., 1985. Determining Lyapunov exponents from a time series. *Phys. Nonlinear Phenom.* 16 (3), 285–317.
- Yates, F.E., Benton, L.A., 1994. "Variance structure in the human cardiovascular system—periodicity, chaos, or old-fashioned noise? *Math. Comput. Model.* 19, 161–170, 6–8.
- Zhang, J.Q., Holden, A.V., Monfredi, O., Boyett, M.R., Zhang, H., 2009. "Stochastic vagal modulation of cardiac pacemaking may lead to erroneous identification of cardiac chaos. *Chaos: Interdis. J. Nonlinear. Sci.* 19 (2), 028509.